Journal of Nanobiotechnology

REVIEW

Open Access

Recent developments in two-dimensional molybdenum disulfide-based multimodal cancer theranostics

Xinbo Yu[1,2†], Chen Xu[1,2†], Jingxu Sun[1†], Hainan Xu[3†], Hanwei Huang[1,2], Ziyang Gan[4], Antony George[4], Sihui Ouyang[5*] and Funan Liu[1,2*]

Abstract

Recent advancements in cancer research have led to the generation of innovative nanomaterials for improved diagnostic and therapeutic strategies. Despite the proven potential of two-dimensional (2D) molybdenum disulfide (MoS_2) as a versatile platform in biomedical applications, few review articles have focused on MoS_2-based platforms for cancer theranostics. This review aims to fill this gap by providing a comprehensive overview of the latest developments in 2D MoS_2 cancer theranostics and emerging strategies in this field. This review highlights the potential applications of 2D MoS_2 in single-model imaging and therapy, including fluorescence imaging, photoacoustic imaging, photothermal therapy, and catalytic therapy. This review further classifies the potential of 2D MoS_2 in multimodal imaging for diagnostic and synergistic theranostic platforms. In particular, this review underscores the progress of 2D MoS_2 as an integrated drug delivery system, covering a broad spectrum of therapeutic strategies from chemotherapy and gene therapy to immunotherapy and photodynamic therapy. Finally, this review discusses the current challenges and future perspectives in meeting the diverse demands of advanced cancer diagnostic and theranostic applications.

Keywords Two-dimensional materials, Molybdenum disulfide, Nanomedicine, Bioimaging, Cancer therapy

†Xinbo Yu, Chen Xu, Jingxu Sun and Hainan Xu contributed equally to this work.

*Correspondence:
Sihui Ouyang
sihuiouyang@cqu.edu.cn
Funan Liu
fnliu@cmu.edu.cn
Full list of author information is available at the end of the article

Graphical Abstract

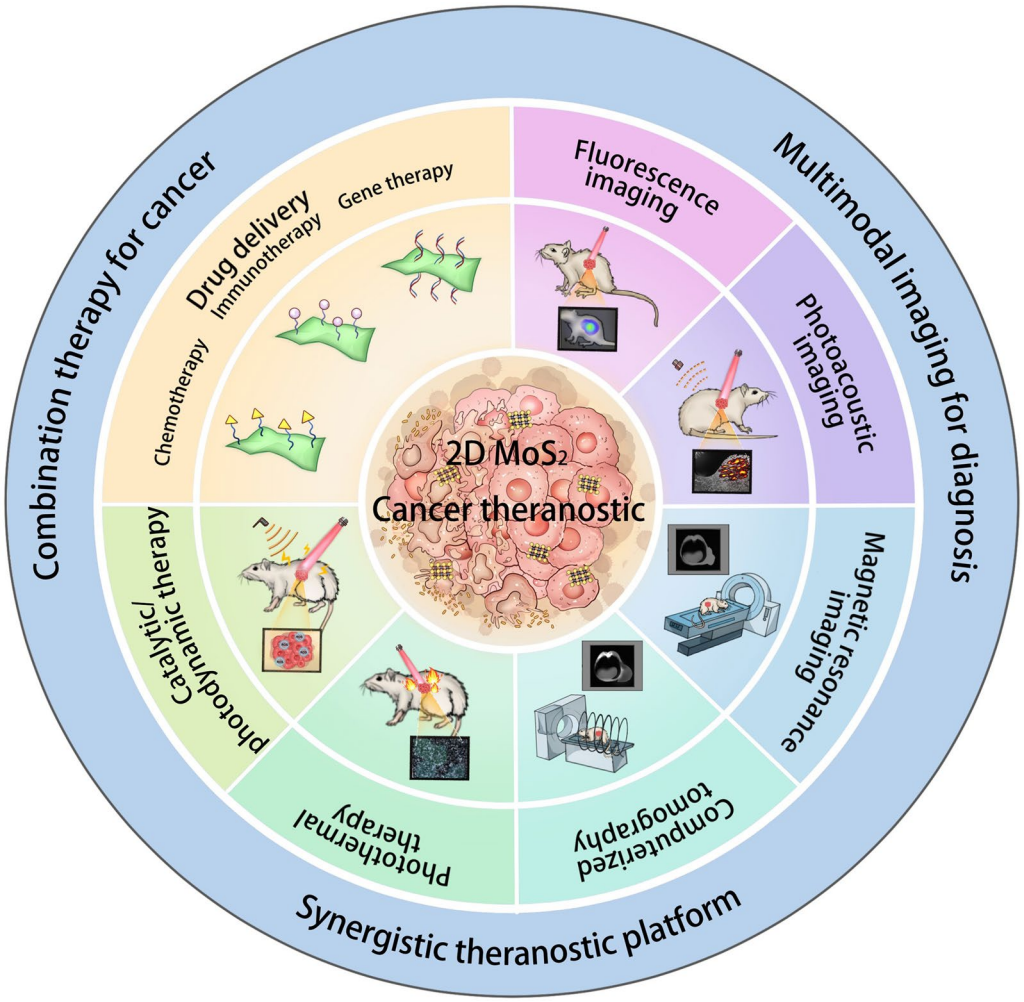

Introduction

In the post-COVID era, the urgency for further advancements in cancer theranostics has become increasingly intense [1, 2]. While conventional therapeutic and diagnostic modalities have benefits, they also have inherent limitations. These limitations include unavoidable adverse reactions due to the nonspecificity of chemotherapy agents, the inability to eliminate micrometastases resulting from the localized nature of surgery and radiation therapy, and the inadequate imaging resolution provided by commonly used contrast agents [3–5]. Consequently, these limitations underscore the urgent need for the development of more efficacious theranostic strategies. Notably, emerging nanotechnologies, particularly two-dimensional (2D) materials, have been positioned at the forefront of research in accelerating cancer theranostics [6, 7]. Among the various 2D materials recently explored, 2D transition metal dichalcogenides (TMDs) stand out for their promising advantages. These advantages include (1) their small size, which allows for the enhanced permeation and retention (EPR) effect [8, 9]; (2) their potential for ensuring biocompatibility, physiological stability and safety [10, 11]; and (3) their high specific surface area, which facilitates the easy loading or delivery of functional molecules, imaging or therapeutic agents, thus combining both imaging and therapeutic functionalities [12–14].

Among all known TMDs, 2D molybdenum disulfide (MoS_2) has garnered considerable attention in the biomedical field because of its exceptional inherent properties [15, 16]. These properties include

photoluminescence (PL) resulting from an indirect bandgap and distinct fluorescence properties; remarkable photothermal properties, such as strong absorption in the near-infrared (NIR) region; an outstanding photothermal conversion rate; enzyme-like catalytic activity; and a potent X-ray attenuation ability attributed to the high atomic number of Mo [17–20]. Consequently, 2D MoS_2 has been utilized in applications such as optical imaging, computerized tomography (CT), photothermal therapy (PTT), and catalytic therapy. Like other 2D nanomaterials, 2D MoS_2 has an ultrahigh surface-to-volume ratio, thereby acting as a versatile nanoplatform to load various agents for tumor treatment [21]. However, challenges such as limited biocompatibility and a propensity to aggregate in physiological environments have restricted the widespread application of conventional 2D MoS_2 [22, 23]. The growing demand for multifunctionality in biomedical fields has necessitated the optimization of 2D MoS_2. Surface modification strategies, involving the introduction of functional molecules such as biocompatible polyethylene glycol (PEG) and targeted folic acid (FA), have been employed to confer increased physiological stability, enhanced biocompatibility, and improved targeting capabilities to 2D MoS_2 [24, 25]. Furthermore, the incorporation of other nanoparticles can provide additional functionality and expand the range of applications for 2D MoS_2. For instance, the attachment of superparamagnetic nanoparticles can endow 2D MoS_2 with magnetic properties, broadening its application in magnetic resonance imaging (MRI) [26].

While still in its nascent stage, the study of 2D MoS_2 has made notable strides in biomedicine in recent years. Given that a comprehensive review of 2D MoS_2 for synergistic applications in imaging, therapy, and drug delivery remains elusive, this review aims to fill that gap by summarizing relevant advancements. In this context, we summarize the synthetic strategies utilized and elucidate the properties retained following surface modification. Furthermore, we emphasize the potential biomedical applications of these properties, with a particular focus on bioimaging and tumor therapy. Future prospects and challenges are also discussed, aiming to chart a course toward the development of more efficacious 2D MoS_2-based cancer theranostic strategies.

Evaluation of 2D MoS_2 performance in nanomedicine

Unlike early 2D materials such as graphene, which is hampered by high toxicity, black phosphorus that is limited by instability, and hexagonal boron nitride that is limited by its insulating nature and lack of strong NIR absorption, 2D MoS_2 displays minimal toxicity and robust chemical stability [27–29]. Its outstanding optical properties, catalytic functionality, and high specific surface area, coupled with the advantages of a small size for drug delivery, show significant potential in cancer theranostics [30]. Additionally, 2D MoS_2 is amenable to scalable, high-quality synthesis, making it a promising candidate for transformation [31]. However, the practical application of 2D MoS_2 in tumor diagnosis and treatment faces considerable challenges. The optimization of synthesis methods is crucial for producing biomedical-grade 2D MoS_2 to increase its clinical scalability. Improvements in therapeutic efficacy and safety are also necessary. These issues can be partially addressed through surface modifications, which can impart greater biocompatibility, physiological stability, and targeting ability to 2D MoS_2 [32]. We evaluate 2D MoS_2 from the perspectives of synthesis, inherent characteristics, and tolerance properties, aiming to align its biomedical specifications with the requirements of cancer theranostics.

Scalability

Different synthetic strategies produce 2D MoS_2 nanomaterials with distinct properties [33]. Currently, various synthesis strategies have been investigated with two main approaches: top-down strategies, including mechanical exfoliation, chemical exfoliation and liquid-phase exfoliation (LPE), and bottom-up strategies, including chemical vapor deposition (CVD) and hydrothermal or solvothermal methods [34–37]. Top-down strategies involve peeling or etching large-sized MoS_2 into mono- or few-layered nanosheets. In contrast, bottom-up strategies refer to the process of assembling small building blocks (atomic or molecular building blocks) into relatively large nanoscale MoS_2 [38]. In the following sections, we briefly describe these classic synthetic methods while considering their feasibility and limitations from a biomedical perspective.

Physical exfoliation, or mechanical exfoliation, is a typical top-down method used to synthesize 2D MoS_2. In this process, a tape and a substrate are usually required to peel and hold thin films, respectively. Due to the weak van der Waals force between layers, 2D MoS_2 is easily exfoliated from a bulk crystal, adhered to the tape, transferred to and retained on the appropriate substrate [39]. The simplicity of the operation and the cleanness of the obtained 2D MoS_2 inspired physical exfoliation as a promising synthetic strategy, but it has not been popularized because the uncontrollability of the peel size or thickness and the low production yield limit its use in biomedical applications [33, 40].

Chemical exfoliation, achieved through the intercalation of ions or molecules, is another method used

to produce 2D MoS_2 [35]. Among various candidates, alkali metals, particularly lithium (Li), are prominent because of their high reduction potential, reactivity, and mobility within the MoS_2 layers [41]. Morrison et al. submerged MoS_2 powder in n-butyllithium to prepare Li ion (Li^+)-intercalated MoS_2. Following the transfer of the intercalated material into water, the Li in the gaps reacts vigorously with the water to evolve hydrogen, resulting in the adjacent layers separating and dispersing in the water [42]. Although high throughput can be achieved by successive intercalation, the conventional Li intercalation method is time-consuming and requires water-free conditions, which limits its universality [38, 43]. Fortunately, some methods, such as microwave/ultrasonication-assisted intercalation, have accelerated the reaction process and improved efficiency [44]. In addition, the toxicity of residual Li^+ is a serious concern, especially in biomedical applications [38]. Therefore, several rational non-Li intercalants, such as potassium ions and ammonia/ammonium ions, have been explored for more secure applications [45, 46]. Importantly, the use of some natural polymers and biomacromolecules, such as chitosan (CS) and bovine serum albumin (BSA), as intercalants could improve the dispersity and biocompatibility of 2D MoS_2 in biological systems [47, 48].

LPE proceeds in three stages: bulk MoS_2 slab dispersion in a specific solvent, ultrasonication, and centrifugation [49]. Due to the acoustic cavitation effects, MoS_2 slabs are successfully exfoliated into nanosheets upon ultrasonication. In addition, appropriate solvents can provide shear force and weaken the interactions between layers, which commits to the preparation of 2D MoS_2 dispersions in collaboration with ultrasonication [50]. However, commonly used dispersants such as N-methylpyrrolidone present challenges in removal because of the strong adsorption mediated by the specific surface energy of 2D MoS_2 and the high boiling point of organic solvents [51, 52]. Not only could this strong adsorption lead to flake deposition, but the toxicity of these solvents limits the broad application of 2D MoS_2, especially in the context of biomedicine [50, 52, 53]. Strikingly, the use of easy-to-remove, low-toxicity or even nontoxic surfactants such as deoxyribonucleic acid (DNA)/ribonucleic acid (RNA) nucleotides has partly solved this problem, achieving the safe and efficient production of nanosheets, especially for biomedical purposes [54].

CVD is a typical bottom-up method for the low-cost and large-scale production of MoS_2 monolayers [55]. In this process, the source materials, generally sulfur powder and Mo-based oxide/chloride, are first sublimated such that the precursor reagents are in the gas state. After being transported through the inert carrier gas, the reactant vapor then diffuses to the substrate and adsorbs onto the substrate surface. The adsorbed atoms (Mo and S) subsequently diffuse along the substrate surface and react with each other to form films [56]. Unfortunately, the difficulty in transferring 2D MoS_2 into physiological solutions and its instability under physiological conditions limit its biomedical applications [38, 57].

As one of the simplest synthesis methods, the hydrothermal/solvothermal method has received much attention. This process involves 2D MoS_2 crystallization from an aqueous/organic solution after the hydrothermal reaction between source materials [58]. Generally, the reaction is conducted in a Teflon-lined stainless-steel autoclave at moderate temperature and high pressure with Mo and S precursor solutions as reactants, which are usually S-containing salt/organic and Mo-containing salt/oxide. As the reaction ends and the reaction system cools down, 2D MoS_2 crystallizes [33, 41]. It is important to note that this preparation method may not be universally applicable, as specific adjustments might be required depending on the reactants and desired properties of the final product. Due to its ability to grow high-quality, uniform, pure and even biocompatible 2D MoS_2 materials, the hydrothermal/solvothermal method has been widely adopted and is the choice in the biomedical field [38, 41]. For instance, with ammonium tetrathiomolybdate as the precursor, Wang et al. prepared PEGylated 2D MoS_2 via a solvothermal reaction in a PEG-400 aqueous solution [24]. Notably, PEGylated nanosheets have high colloidal stability and biocompatibility, indicating their excellent application value in biomedicine.

Scalability is a crucial factor when considering practical clinical applications. The synthesis of 2D MoS_2 must be feasible on a large scale while maintaining consistency and quality. Chemical exfoliation offers higher throughput, especially with advancements such as microwave/ultrasonication-assisted intercalation, which improve the efficiency and scalability [35]. LPE is also scalable, particularly when nontoxic surfactants are used to simplify solvent removal and reduce toxicity, making it viable for industrial applications [54]. CVD can produce large-area 2D MoS_2 at low cost and is suitable for industrial applications, although it requires modifications for stability in physiological solutions [55]. The hydrothermal/solvothermal method is noted for its ability to produce high-quality, uniform 2D MoS_2 under moderate conditions, making it cost-effective and highly efficient for large-scale production [41]. Thus, CVD and hydrothermal/solvothermal methods are promising for scalable production for consistent and reproducible

theranostic applications, while improved chemical exfoliation and LPE techniques also show potential.

Toxicity and biosafety

To date, toxicity remains a critical obstacle hindering the widespread application of 2D nanomaterials. Even though 2D MoS_2 is less hazardous than some other materials, such as graphene and its analogs, its toxicity cannot be overlooked [59, 60]. To this end, toxicological studies have demonstrated that 2D MoS_2 has mild toxicity, which is primarily linked to increased oxidative stress and physical disruption. Oxidative stress is a major contributor to nanotoxicity, such as organelle damage and cell death [61]. A study of Kupffer cells revealed that the dissolution of nanosheets and the release of hexavalent Mo contribute to mitochondrial reactive oxygen species (ROS) generation, inducing caspase 3/7-mediated apoptosis. This effect is dose dependent, with statistically significant reductions in cell viability observed at concentrations greater than 25 μg/mL [62]. Importantly, even chronic low-dose (1 μg/mL) exposure (7 days) can induce severe toxic effects. HaCaT keratinocytes exhibited a loss of cell membrane integrity, mitochondrial dysfunction, endoplasmic reticulum (ER) disorder, and nuclear damage after chronic exposure. These changes are attributed to the disruption of cell membrane integrity due to high cellular internalization and increased oxidative stress caused by faster electron transfer from MoS_2, which seizes electrons from the mitochondrial membrane, disturbing normal electron transport. The function of cell organelles is subsequently compromised, resulting in a failure to maintain normal metabolic activity [63]. ROS generation induced by chemically exfoliated MoS_2 also mediates DNA cleavage, another key mechanism of nanotoxicity [64]. In addition to oxidative stress induction, 2D MoS_2 can directly cause physical damage to cells and organelles. For example, the internalization of 2D MoS_2 disrupts cell membrane integrity, as mentioned above [63]. The 2D MoS_2 can penetrate the mitochondrial lipid membrane through hydrophobic interactions, causing heterogeneous lipid packing and resulting in damage [65]. In addition to intrinsic toxicity, the distribution state of 2D MoS_2 is also a significant factor influencing its toxicity. Wang et al. showed that aggregated MoS_2 induced strong proinflammatory and profibrogenic responses in vitro and acute lung inflammation in mice, whereas exfoliated MoS_2 had little or no effect [22]. This finding underscores the importance of further modification and functionalization not only to increase the biocompatibility of 2D MoS_2 itself but also to reduce aggregation and increase physiological stability to improve safety.

Given that the inherent toxicity of 2D MoS_2 and damage, such as inflammation caused by nanosheet aggregation, can highlight the concern of wide bioapplication and clinical translation, optimizing the biocompatibility and physiological stability of 2D MoS_2 remains essential [22, 62, 66]. In this respect, many polymers or biomimetic molecules, such as PEG, CS and lipids, have been extensively used to functionalize 2D MoS_2 for increased biosafety. PEG is considered the preferred polymer in drug delivery systems because of its structural flexibility, amphiphilicity, and especially well-established safety profile [67]. Hao et al. prepared MoS_2-PEG by anchoring lipoic acid-conjugated PEG (LA-PEG) to the surface defect sites of 2D MoS_2 via Mo-S bonding [68]. As expected, PEG provided 2D MoS_2 with enhanced biocompatibility. Severe toxicity in vitro and in vivo was not detected even at high concentrations, and further long-term toxicity within a reasonable dose range could be neglected in light of the almost complete clearance of MoS_2-PEG within 30 d. Remarkably, PEGylation also greatly increased the physiological stability, with MoS_2-PEG being fairly stable in diverse physiological solutions, including RPMI-1640 medium, phosphate-buffered saline (PBS), and fetal bovine serum. On the other hand, CS, a natural and abundant biopolymer, is usually used as a biocompatible agent [69]. Yin et al. introduced CS to the surface of 2D MoS_2 via physical interactions to synthesize MoS_2-CS [70]. MoS_2-CS nanosheets are well dispersed in water and other physiological buffers and exhibit greater physiological stability and biocompatibility than MoS_2. Lipids have emerged as excellent candidates for surface coatings because of their ability to improve the solubility of drugs, their biodegradability, and their biocompatibility [71]. Building on this foundation, Xie et al. developed MoS_2-lipid nanocomposites [72]. Lipid modification significantly improved the stability and biocompatibility of 2D MoS_2. Unlike untreated MoS_2, which exhibited severe coagulation in water, PBS, and cell culture media over 48 h, MoS_2-lipid maintained excellent dispersibility and stability in all three environments. Additionally, lipid modification increased the hydrophilicity of MoS_2, resulting in a much lower BSA adsorption rate than that of unmodified MoS_2, thus indicating the enhanced biocompatibility of MoS_2-lipid.

Targeting

As targeting is the functional basis of efficient and safe tumor diagnosis and treatment, achieving precise targeting should always be our goal [73]. Due to the small size of ordinary 2D MoS_2, targeting is achieved primarily through the EPR effect, also referred to as passive targeting [74]. Furthermore, modification with

adaptive biological molecules such as PEG can enhance the passive targeting capability of 2D MoS_2. This expectation is reasonable since PEGylation helps reduce reticuloendothelial system uptake, thus improving accumulation in the tumor [75]. However, relying solely on the EPR effect is inadequate in practice, whereas smart and precise targeting is sought. This demand has encouraged the development of active targeting and response targeting methods based on high-specificity targeting ligands and sensitive stimulus-responsive elements, respectively [76, 77]. Currently, targeting ligands, including peptides such as arginine–glycine–aspartate (RGD) and small molecules such as FA and hyaluronic acid (HA), have been widely utilized to decorate 2D MoS_2 [78–80]. The corresponding receptors are typically overexpressed on tumor cells instead of healthy cells, thereby presenting tumor specificity and conferring tumor targeting to 2D MoS_2. For example, RGD selectively binds to αvβ3 integrin, which is commonly overexpressed in tumor cells such as HeLa cells. Additionally, the FA receptor is upregulated in various types of epithelial cancers and 90% of ovarian carcinomas and is expressed at low levels in healthy tissues. HA can specifically bind to cluster determinant 44 (CD44), which is overexpressed on various tumor cell surfaces. Guided by these ligands, 2D MoS_2 attaches to tumor cells expressing the corresponding receptors for internalization, enabling improved targeting and bioavailability [81, 82]. In another dynamic targeting strategy, 2D MoS_2 is modified with responsive molecules or chemical bonds such as HA and disulfide bonds (S–S). These modifications respond to internal (pH, enzymes, redox, etc.) or external (light, heat, ultrasound, etc.) stimuli for effective targeting [80–83]. For example, hyaluronidase and glutathione (GSH), which are abundant in the tumor microenvironment (TME) but absent in normal tissues, can efficiently cleave HA and reduce S–S. This property endows 2D MoS_2 with responsive targeting and the precise release of loaded substances from MoS_2-HA or MoS_2-SS as carriers.

Approaches for single-mode imaging and therapy

The early diagnosis of cancer and subsequent effective therapies are undeniably critical for a good prognosis [84]. Various noninvasive bioimaging techniques, such as MRI, photoacoustic imaging (PAI), and fluorescence imaging (FI), can be employed for early diagnosis [85–87]. Through the development of tailored imaging agents, these powerful techniques have demonstrated efficacy in the identification and characterization of diseases in their nascent stages [88]. Due to their unique optical and photothermal properties and additional or enhanced characteristics conferred by loading, 2D MoS_2 and its compounds have displayed immense potential in these imaging modalities as imaging agents. In addition to imaging applications, 2D MoS_2 is also a promising therapeutic agent for cancer treatment, especially as a photothermal agent (PTA), due to its excellent photothermal properties [57]. Furthermore, 2D MoS_2 has been investigated as an outstanding catalyst for therapeutic interventions because of its high surface area, abundant defects, and sulfur vacancies [89, 90]. In this work, we present the advantages of 2D MoS_2 in approaches for single-mode imaging and therapy, including FI, PAI, PTT and catalytic therapy.

2D MoS_2 in fluorescence imaging

FI has attracted considerable interest and has emerged as a rapidly evolving and promising imaging method in the biomedical context [91]. Its attractiveness lies in its high sensitivity, impressive resolution, quick feedback, and substantial safety due to its noninvasive nature and absence of ionizing radiation [92, 93]. These advantageous characteristics have positioned FI as an indispensable tool in the exploration of various biological phenomena. Notably, the unique inherent PL or fluorescence characteristics of 2D MoS_2 make them an optimal choice for FI. Building on these findings, Qi et al. utilized 2D MoS_2 as a fluorescent label for imaging HepG2 cells [94]. Their experiments revealed a crucial finding: numerous 2D MoS_2 molecules with strong fluorescence were internalized into cells. When the cells were irradiated with broad-band excitation light, specifically UV (300–400 nm), blue (400–500 nm), and green (500–600 nm) light, the fluorescently labeled cells appeared blue, green, and red, respectively, in the fluorescence images. The cells exhibited vibrant colors corresponding to the specific wavelength of light used, which allowed easy differentiation. Additionally, they showed clear morphologies in the bright field image, highlighting the effectiveness of 2D MoS_2 as a tool for detailed cellular studies.

Theoretically, coupling these strongly fluorescent 2D MoS_2 with fluorescent dyes may result in a dual fluorescence effect. More importantly, the use of 2D MoS_2 as a carrier enhances the accumulation of fluorescent dyes through the EPR effect, thereby potentially generating greater effectiveness. Unfortunately, the fluorescence emission quenching or decreasing property of 2D MoS_2 renders that phenomenon invalid [95]. Wang et al. solved this problem to some extent through an "intermediary" strategy [96]. In this frontier work, MoS_2-PEG was embedded into mesoporous silica nanoparticles (MSNs), playing the role of an "intermediary", and then the aggregation-induced emission fluorogen $PhENH_2$ was chemically grafted onto the MSNs, triggering

robust fluorescence emission (Fig. 1A, B). FA was also linked to the surface of the MSNs, leading to the synthesis of $PhENH_2$-MoS_2-FA MSNs. Interestingly, after an incubation with $PhENH_2$-MoS_2-FA MSNs, MDA-MB-231 cells, which highly express FA receptors, exhibited potent red fluorescence. This fluorescence intensity notably surpassed that of HepG2 cells, which lack FA receptors, emphasizing the targeting efficacy of these nanoparticles.

In addition to directly targeting tumor cells for imaging, 2D MoS_2 can also be used for molecular detection imaging, allowing researchers the ability to distinguish tumor cells from normal cells. Due to oxidative metabolism disorders, more hydrogen peroxide (H_2O_2) accumulates in tumor cells than in normal cells [97]. These findings indicate that H_2O_2 and H_2O_2-induced oxidative stress could serve as markers for tumor cells. Based on this information, Liu et al. layered 2D MoS_2 with ortho-phenylenediamine (OPD) to quantify the intracellular concentrations of H_2O_2 and thus distinguished cells under pathological conditions [98]. During this procedure, 2D MoS_2, which possesses

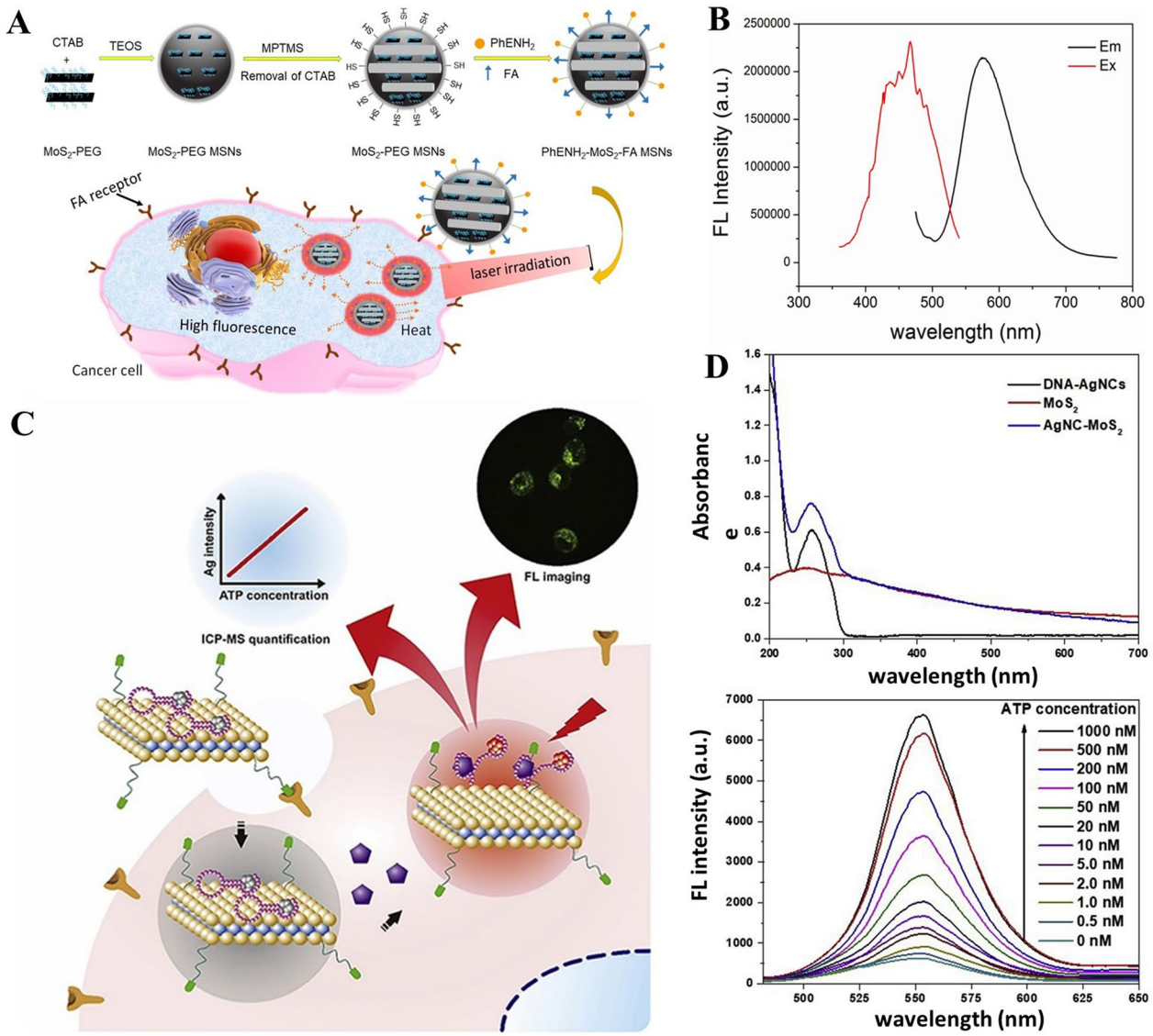

Fig. 1 **A** Schematic diagram of the preparation of $PhENH_2$-MoS_2-FA MSNs and their fluorescence effect. **B** Fluorescence spectra of $PhENH_2$-MoS_2-FA MSNs dispersed in water. **C** Schematic diagram of the sensing principle of AgNC@MoS_2 probe. **D** UV–Vis absorption spectra and synchronous scanning fluorescence spectra of AgNC@MoS_2 probe. Reproduced with permission [96]. Copyright 2019, Elsevier. Reproduced with permission [102]. Copyright 2020, Elsevier

high peroxidase (POD)-mimicking catalytic activity, decomposed H_2O_2 into hydroxyl radicals (OH·) to oxidize OPD. The resulting OPD oxide then emitted fluorescence with a maximum at ~ 557 nm upon excitation at 450 nm. This light emission characteristic enabled a clear distinction between human foreskin fibroblasts and HeLa cells via intensity feedback (the fluorescent signal was low for the former but higher for the latter) [98, 99].

Although the fluorescence quenching property of 2D MoS_2 is regrettable on direct imaging, as mentioned above, encouragingly, this property is used in the "switching" strategy to provide a higher target-to-background ratio for FI. Briefly, the use of 2D MoS_2 as a quencher maintains the fluorescence in an "off" state in circulation, while the signal turns to an "on" state with the degradation of nanoparticles mediated by some specific molecules and the consequent release of the dye at the target site [100]. Building on this strategy, Jia et al. grafted an adenosine triphosphate (ATP) aptamer (Apt)-labeled photosensitizer, chlorine e6 (Ce6), onto 2D MoS_2 for intracellular ATP imaging. Upon internalization into cancer cells, these compounds accumulate in ATP-rich lysosomes. Here, the intracellular ATP binds to the Apt, resulting in the release of Ce6-Apt and consequently the restoration of Ce6 fluorescence [101]. Furthermore, Xu et al. synthesized a AgNC@MoS_2 probe by assembling fluorescent DNA-silver nanoclusters (DNA-AgNCs) with the ATP Apt as a template and LA-PEG-FA on 2D MoS_2 (Fig. 1C) [102]. This method allows positive targeting imaging and a quantitative analysis of intracellular ATP concentrations (Fig. 1D). In practical terms, when AgNC@MoS_2-PEG-FA is taken up by tumor cells overexpressing the FA receptor, the recognition of ATP by the probe triggers the release of DNA-AgNCs and the recovery of fluorescence. The released DNA-AgNCs can be measured via inductively coupled plasma–mass spectrometry. This step is crucial, as it provides accurate quantitative information and enables a quantitative analysis of intracellular ATP concentrations. In summary, 2D MoS_2 offers significant potential for direct cellular imaging and molecular monitoring. However, the application of 2D MoS_2 in clinical FI remains elusive primarily due to the need for enhancements in brightness, photostability, and safety, necessitating further effectiveness and biocompatibility modifications.

2D MoS_2 in photoacoustic imaging

As an emerging imaging modality, PAI has attracted much attention because of its excellent superiority with respect to higher resolution than traditional MRI, deeper penetration than optical imaging, and lack of radiation exposure [103, 104]. When exposed to pulsed light, instant thermoelastic expansion occurs in the photoabsorption tissue and creates an ultrasound wave, which is subsequently detected by an ultrasonic transducer and converted into an image [105]. Benefiting from the pronounced light absorbance, high photothermal conversion rate, ability to produce ultrasonic waves and exceptional resolution improved by the generation of air microbubbles, 2D MoS_2 is believed to be a promising contrast agent for PAI [12, 106]. In this context, Chen et al. prepared single-layer 2D MoS_2 nanosheets and explored their potential for augmenting photoacoustic (PA) signals [107]. The nanosheets were efficiently internalized into glioma cells. This internalization resulted in strong PA signals with an impressively sensitive detection limit of approximately 100 cells. Encouraging outcomes were also observed in subcutaneous and orthotopic tumor-bearing mice. The tumor tissue nearly 1.5 mm below the skull was clearly visualized. Nevertheless, relying solely on simple 2D MoS_2 when encountering gliomas at even deeper sites is insufficient, necessitating the utilization of more advanced contrast agents. For this reason, Liu et al. introduced indocyanine green (ICG), a dye with a high NIR extinction coefficient, onto the surface of 2D MoS_2, obtaining MoS_2-ICG with higher sensitivity [108, 109]. This adjustment provided clear benefits. The absorption peak (800 nm) of MoS_2-ICG was significantly greater than that of 2D MoS_2 (675 nm). This shift allowed PAI to be conducted at longer wavelengths, which could lower the background noise and increase the penetration depth. Remarkably, the PA signal observed upon 800 nm laser excitation of MoS_2-ICG was approximately 16-fold greater than that of MoS_2. This enhancement exhibited a concentration-dependent profile and was coupled with outstanding photostability. In practice, this enhancement translated to an impressive imaging depth of up to 3.5 mm when MoS_2-ICG was used for in vivo PAI of orthotopic gliomas in the brain. This depth was almost twice that achieved using 2D MoS_2, suggesting the significant potential of MoS_2-ICG in PAI applications. In summary, the advancements obtained in PAI applications using 2D MoS_2 and MoS_2-ICG highlight the critical role of contrast agents in enhancing the capabilities of PAI. While 2D MoS_2 shows remarkable efficacy in visualizing tumor tissues near the surface, its limitations at greater depths necessitate the exploration of modified agents such as MoS_2-ICG. This finding underscores the importance of continuous optimization to meet demands for higher-resolution imaging, particularly in deep tissue imaging.

2D MoS_2 in photothermal therapy

PTT is a technique that utilizes the principle of converting absorbed light into heat, thereby inducing

thermal damage in the tumor [110]. In this process, PTAs possess excellent photothermal properties and safety and are critical factors for achieving high therapeutic efficacy [111]. Among various PTAs, 2D MoS_2 stands out because of its admirable optical absorption, photothermal conversion efficiency, and biocompatibility.

In a recent study, Chen et al. synthesized PEGylated MoS_2 nanosheets (MoS_2-PPEG) with poly(acrylic acid) (PAA), resulting in the ability of the obtained nanosheets to degrade (Fig. 2A) [112]. Notably, the MoS_2-PPEG demonstrated exceptional stability and photothermal properties. For example, upon 300 s of NIR laser irradiation, the temperature of the MoS_2-PPEG dispersion at a concentration of 200 μg/mL increased from 25.8 to 51.4 °C, whereas the corresponding temperature change for water was only 1.3 °C. In subsequent in vivo investigations, the temperature of MoS_2-PPEG reached 52.1 °C, whereas the temperature of PBS increased approximately 1 °C. Intriguingly, while the tumor volume of the mice treated with MoS_2-PPEG or NIR laser irradiation alone continuously increased throughout the detection period, PTT with MoS_2-PPEG dramatically suppressed tumor growth (Fig. 2B). Moreover, the body weights of the mice remained stable throughout the treatment period, suggesting a high tolerance to PTT (Fig. 2C).

Enhanced targeting modifications have been engineered to ensure high specificity in recognizing and efficiently targeting tumor cells. Nucleic acid Apts, which are single-stranded oligonucleotides, exhibit excellent

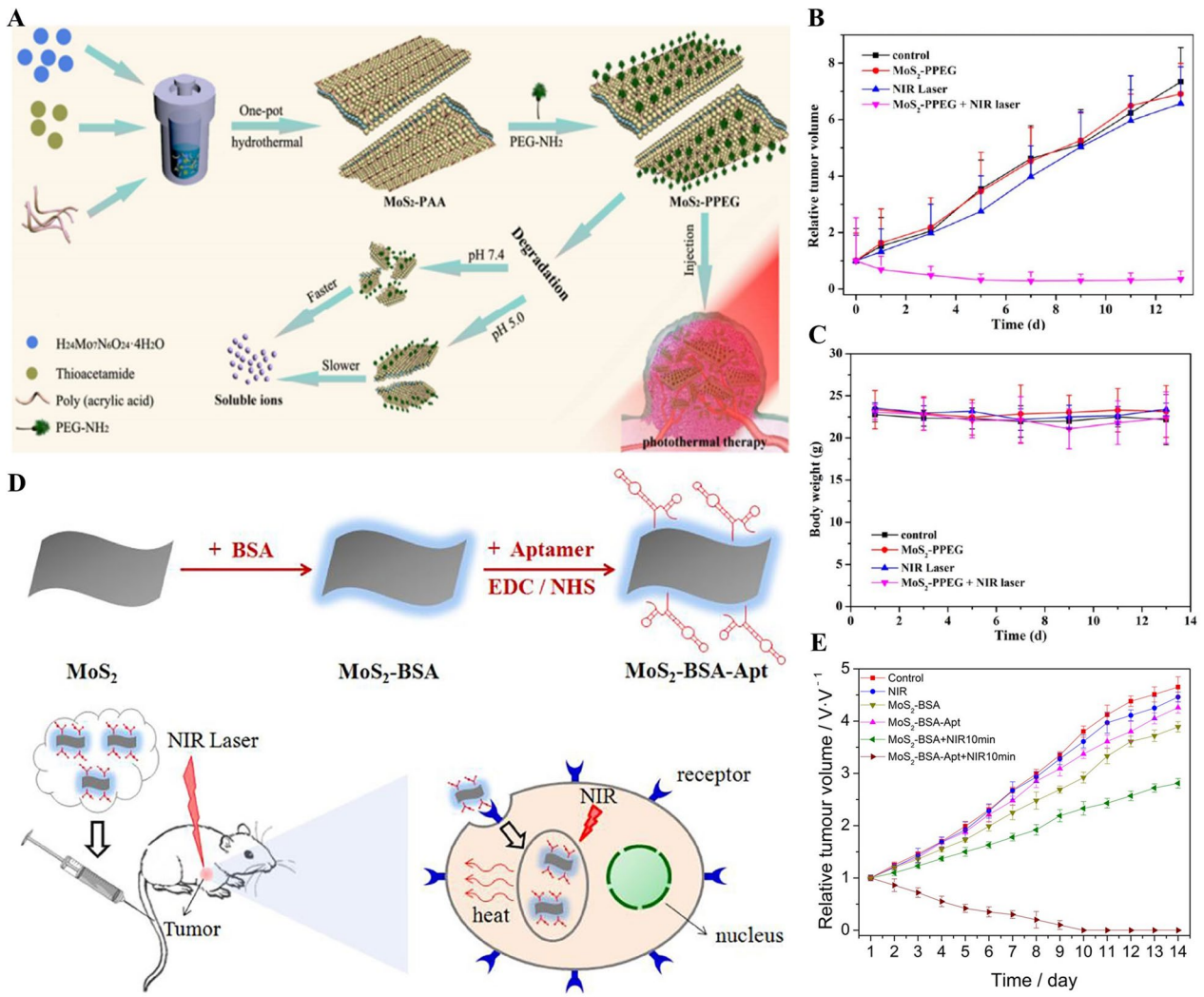

Fig. 2 **A** Schematic diagram of MoS_2-PPEG preparation and in vivo PTT. Relative tumor volume (**B**) and body weight (**C**) of mice under different treatments. **D** Schematic diagram of precise PTT with APT modified 2D MoS_2. **E** Relative tumor volume of mice under different treatments. Reproduced with permission [112]. Copyright 2017, American Chemical Society. Reproduced with permission [114]. Copyright 2021, Elsevier

specificity and affinity for their target molecules [113]. In related work, Pang et al. modified 2D MoS_2 with amino-nucleic Apt and BSA, creating MoS_2-BSA-Apt noted for its precise targeting ability and favorable biocompatibility (Fig. 2D) [114]. When exposed to 808 nm NIR laser irradiation, these nanosheets demonstrated a potent ability to ablate tumors. Remarkably, following the injection of MoS_2-BSA-Apt and subsequent 808 nm laser irradiation for 10 min, the breast tumors in the mice were entirely eliminated after 14 days of PTT. This finding contrasted sharply with the outcomes observed in mice treated with 2D MoS_2 and laser irradiation alone, which failed to effectively inhibit the growth of tumors (Fig. 2E). Furthermore, Liu et al. prepared CD44-targeted 2D MoS_2, referred to as the MoS_2@protein A@CD44 antibody (Ab) [115]. This complex was achieved by coating anti-CD44 Ab on the 2D MoS_2 surface through the connection of a layer of Protein A mixed with bovine BSA. Upon cellular uptake, CD44-targeted MoS_2 led to the depletion of membrane CD44 in lysosomal degradative compartments, resulting in a decrease in RhoA activation (GTP-RhoA) and its downstream epithelial–mesenchymal transition (EMT)-related transcription factors, thereby weakening tumor progression. This result was also expected, as CD44 is known to induce the EMT, a process during which tumor cells lose their original epithelial phenotype and acquire a mesenchymal phenotype characterized by increased stemness, chemoresistance, and invasiveness [116]. Moreover, PTT utilizing MoS_2@CD44Ab induced an increase in the intracellular temperature, which disrupted the activation of these signals and further hampered the biological behavior of the tumor.

Enhanced photothermal therapeutic efficacy is anticipated with the combination of additional PTAs and 2D MoS_2, with the potential of heterojunction architectures to enhance the efficient separation and migration of photoexcited charges [117]. Carbon dots (CDs) have been extensively investigated due to their advantages, such as their excellent safety profile and tunable photochemical properties [118]. Despite the lower photothermal efficiency of CDs, their heterojunctions combined with 2D MoS_2 have exhibited a markedly enhanced photothermal effect compared with that of single 2D MoS_2. Expanding on this concept, Geng et al. reported 0D/2D/0D sandwich heterojunctions, such as NIR-CD/MoS_2, with 0D-N-doped CDs and 2D MoS_2 nanosheets [119]. The results revealed that the absorbance and photothermal conversion efficiency were remarkably greater than those of the pristine NIR-CDs and MoS_2. This enhanced performance was also evident in in vivo studies, where the temperature of the tumors in the NIR-CD/MoS_2 group rapidly increased upon exposure to 808 nm laser irradiation, resulting in complete inhibition of 4T1 tumor growth and no occurrence of pulmonary metastatic nodules at an ultralow power density. Conversely, the tumors in the saline, single NIR-CD/MoS_2, and saline with laser irradiation groups rapidly increased in size within 18 days, and a considerable number of metastatic nodules was observed. Collectively, these examples exemplify the satisfactory efficacy of 2D MoS_2 and its nanocomposites in PTT. Each study contributes uniquely to the field, either through advancements in biocompatibility modifications, targeting strategies, or the development of new heterojunction architectures. Future research should continue to explore additional optimizations, further improving the therapeutic outcomes of PTT.

2D MoS_2 in catalytic therapy

Nanocatalytic therapy has recently emerged as a promising alternative for tumor treatment, leveraging nanozymes to induce catalytic reactions in vivo that generate abundant ROS. These ROS have the potential to significantly impair and even annihilate malignant cells [120]. Among these nanozymes, 2D MoS_2, which functions similarly to POD, offers a stable and cost-effective platform for catalytic activity with outstanding and adjustable catalytic activity in vivo [121, 122].

Recently, Wang et al. highlighted an innovative nanocatalyst, BTO/MoS_2@CA, which responds to the acidic conditions of the TME and is activated by ultrasound (Fig. 3A) [123]. This nanocatalyst is constructed from few-layer MoS_2 nanosheets grown on the surface of piezoelectric tetragonal barium titanate (T-BTO) and is further modified with pH-responsive cinnamaldehyde (CA). In the acidic TME, CA initiates the breakdown of endogenous molecules to release substantial quantities of H_2O_2. The generated H_2O_2 is subsequently transformed into OH· through a series of reactions catalyzed by POD-like BTO/MoS_2 (Fig. 3B). The effectiveness of this reaction is influenced by the ultrasound-induced microscopic pressure, which segregates the positive and negative charges generated by BTO, thereby increasing the interaction between MoS_2 and H_2O_2 and leading to continuous OH· production (Fig. 3C). Furthermore, MoS_2 contributes to the depletion of GSH in cancer cells, intensifying oxidative stress. This stress reduces the levels of GSH-POD-4, disrupting the redox balance and inducing tumor cell ferroptosis (Fig. 3D). The in vivo studies underscore the superior antitumor efficacy of BTO/MoS_2@CA under ultrasound. Compared with the control groups treated with PBS and CA + ultrasound, the BTO/MoS_2@CA + ultrasound group exhibited significant tumor growth inhibition, characterized by pronounced tumor

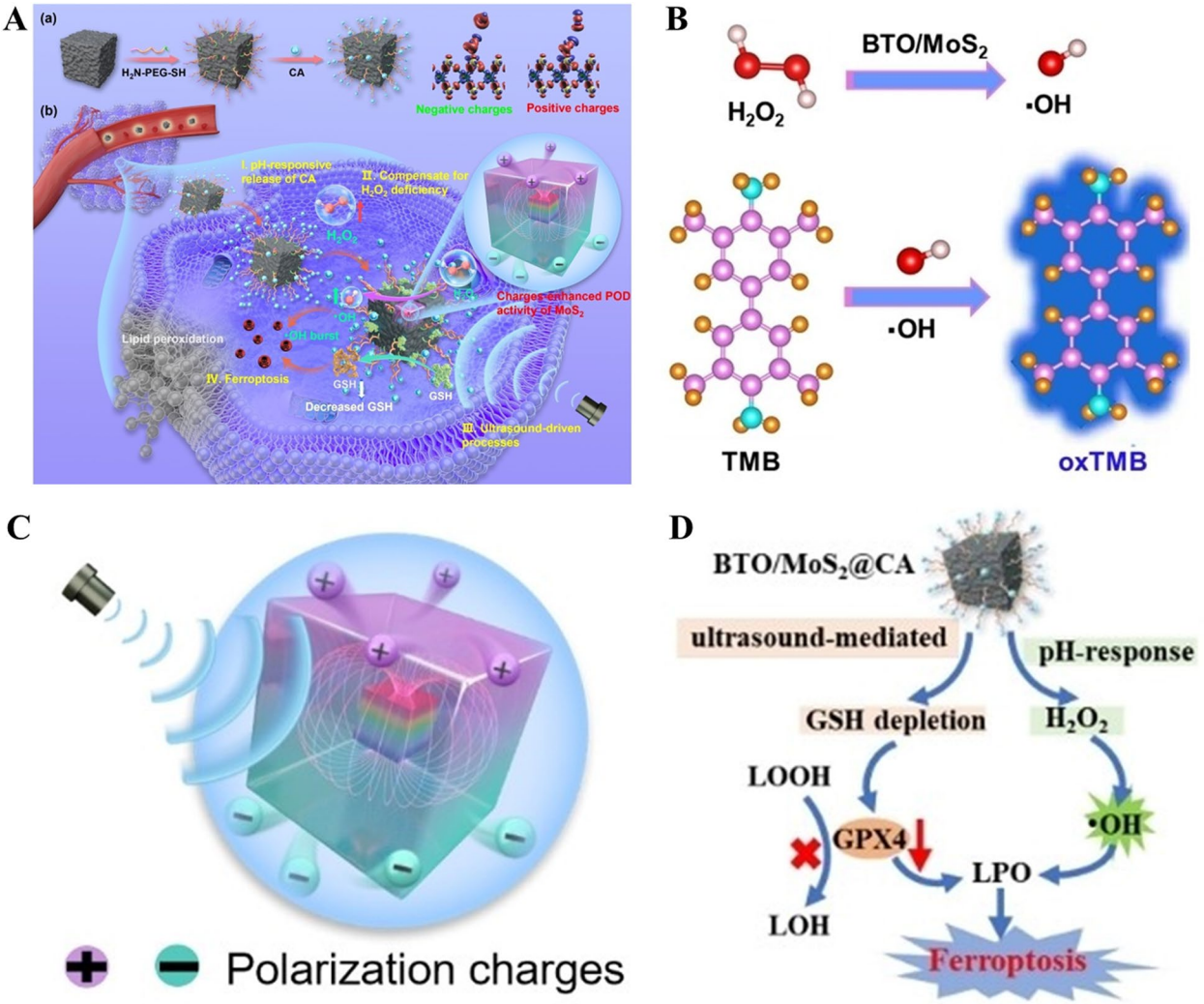

Fig. 3 **A** Schematic diagram of BTO/MoS_2@CA catalytic activity for tumor treatment. **B** Reaction scheme for H_2O_2 decomposition and TMB oxidation. **C** Schematic illustration of the surface positive and negative charges distribution of BTO driven by ultrasound. **D** Schematic diagram of ferroptosis mediated by BTO/MoS_2@CA. Reproduced with permission [123]. Copyright 2023, Wiley

necrosis, hemorrhage, and infiltration of inflammatory cells.

The high specific surface area and abundant surface active sites of 2D MoS_2 facilitate its role as a cocatalyst support for single-atom catalysis, increasing its potential in cancer catalytic therapy [124]. In this context, Yang et al. developed a 2D composite nanocatalyst, termed MoS_2@SA-Fe-PEG (MSFP), by integrating atomically dispersed iron (Fe) onto a MoS_2 support and modifying the surface with amine-polyethylene glycol (NH_2-PEG) [125]. This configuration harnesses the Fenton reaction, a well-known Fe-mediated redox process, to decompose H_2O_2 into OH· at the atomic level [126, 127]. The doped Fe atoms catalyze Fenton reactions, while the abundant sulfur vacancy defects generated on both the flat surface and edge of the nanosheet after Fe doping increase the surface electron density and thereby favor electron capture by H_2O_2 to promote OH· production. Importantly, the MoS_2 support serves as a cocatalyst, enhancing the reduction of Fe^{3+} to Fe^{2+} through its Mo^{4+} sites, thereby facilitating the Fenton process efficiently. Comparative studies underscore the superior catalytic anticancer capabilities of MSFP to traditional nanocatalysts. In contrast to the control group (Fe^{2+} or MoS_2-PEG treatment), which exhibited significant tumor proliferation, the MSFP-treated group displayed distinct tumor suppression and prolonged lifetimes [125]. These studies illustrate significant advancements in the field of

nanocatalytic therapy using 2D MoS_2-based nanozymes. As an emerging field, this topic warrants further in-depth research, including enhancing the catalytic efficiency, selectivity, specificity, and biocompatibility of these nanozymes. Future research should focus on the interplay between their intrinsic structures and external environments to optimize these systems and improve their safety and efficacy in clinical settings [128].

Synergistic strategies in imaging and therapy

Despite recent achievements in cancer diagnosis and treatment, single imaging modalities and therapies often lack the required diagnostic precision and therapeutic efficacy, indicating a strong desire to realize multimodal imaging (MMI), combination therapy, and even highly integrated platforms [129–131]. In particular, due to its large surface area and fascinating photochemical properties, 2D MoS_2 was developed as a promising platform for MMI and cancer treatment.

2D MoS_2 in multimodal imaging

Importantly, limitations remain for each single imaging modality that must be improved, such as the restricted tissue penetration of optical techniques, the radioactivity of CT, and the low sensitivity of MRI [132]. Fortunately, MMI, which is founded on the aforementioned modalities, takes the best out of the worst, whereby the integration of unique strengths and the remedy for each other's shortcomings provide novel insights toward improving the imaging capability [130]. In this regard, as a promising contrast agent, 2D MoS_2 is adaptable to multiple imaging methods simultaneously, leading to more possibilities for the advancement of MMI.

Indeed, numerous MMI methods that combine two or more imaging techniques, such as FI, CT, MRI and PAI, have been extensively investigated in recent years [130, 133]. Among these methods, the dual imaging technique based on 2D MoS_2 has tremendous potential, considering the diverse combinations of intrinsic properties, such as excellent fluorescence properties and photothermal properties, and has emerged as a representative approach in MMI [134, 135]. For example, the dual-modality platform of MoS_2-HA can serve as a fluorescer and PA contrast agent with both fluorescence and PAI capabilities (Fig. 4A) [136]. Subsequent in vivo bioimaging experiments revealed that the fluorescence

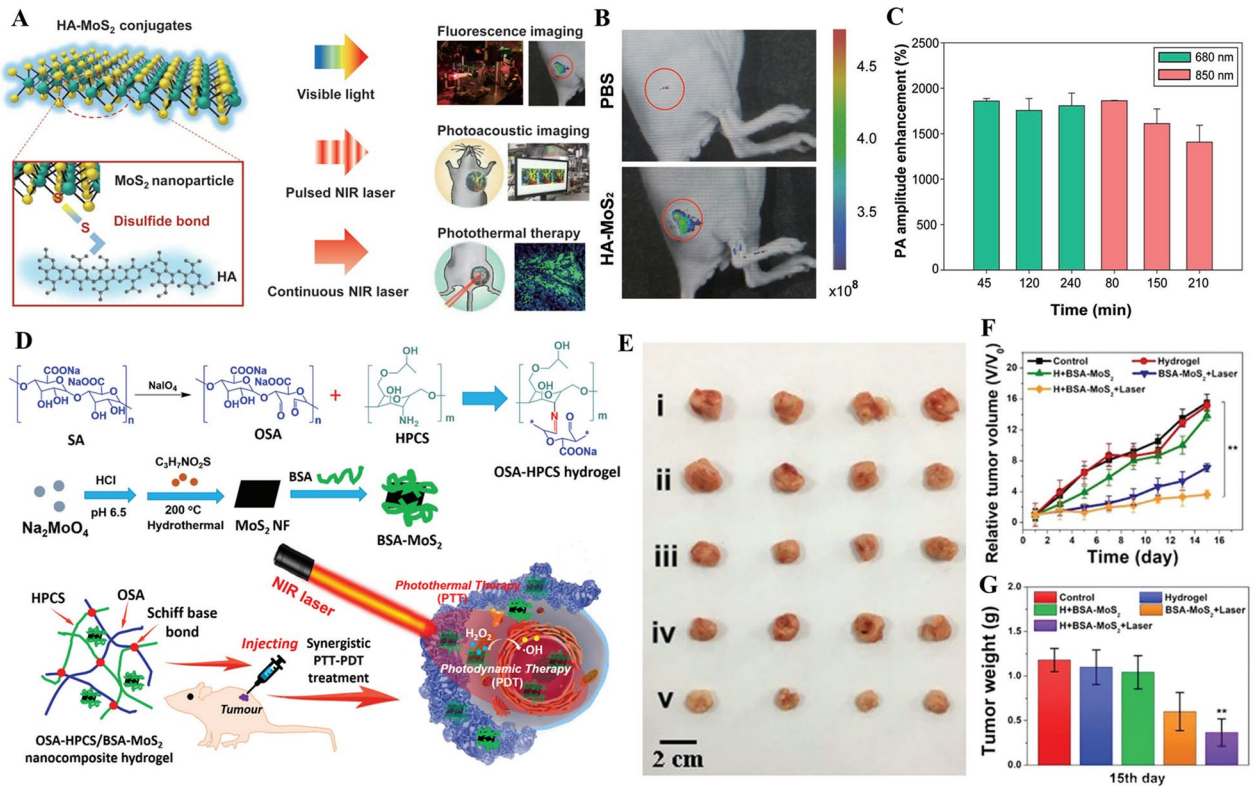

Fig. 4 **A** Schematic diagram of theranostic HA-MoS_2 conjugates. **B** In vivo fluorescence imaging of HA-MoS_2 conjugates. **C** The PA amplitude enhancement of HA-MoS_2 conjugates compared to the control (PBS). **D** Schematic diagram of hydrogel loading MoS_2 nanosheets preparation and synergistic PTT/PDT for cancer. Tumor photographs (**E**), relative tumor volume (**F**) and body weight (**G**) of mice under different treatments. Reproduced with permission [136]. Copyright 2018, Wiley. Reproduced with permission [143]. Copyright 2022, Wiley

signal from MoS_2-HA was markedly observable in the primary tumor (Fig. 4B). In terms of the PA signals, MoS_2-HA demonstrated an astounding 1860-fold increase on average compared with that of PBS, far exceeding the several 100-fold enhancements achieved by traditional PA agents (Fig. 4C) [136, 137].

In addition, by leveraging its strong fluorescence quenching ability and broad absorption in the NIR region, 2D MoS_2 has emerged as a versatile candidate for FI quenchers and PAI contrast agents, enabling multimodal molecular detection and imaging. Li et al. introduced an activatable nanoprobe (MoS_2@ polydopamine (PDA)-PEG/peptide, MPPF) engineered for dual-mode near-infrared fluorescence (NIRF)/ ratiometric PAI to detect endogenous furin activity [138]. The 2D MoS_2 undergoes a coating process with PDA and PEG, after which it is covalently functionalized with Cy7-labeled furin substrate peptides. The enzymatic cleavage of these peptides by furin triggers the release of Cy7 molecules from the MPPF nanoprobes, thereby restoring their fluorescence. Concurrently, this process disrupts the fluorescence resonance energy transfer from Cy7 to MoS_2 and facilitates the efficient removal of small Cy7 molecules from tumor tissues, resulting in a prompt decrease in the PA signal at 768 nm (PA768). In contrast, the PA signal at 900 nm (PA900), attributed to 2D MoS_2, decreases gradually due to its substantial size and slow tumor clearance. This coordinated alteration in NIRF and ratiometric PA signals thus represents a novel method for the real-time visualization of endogenous furin activity. These examples underscore the critical role of 2D MoS_2 as a MMI platform in advancing the precision of biomedical imaging and overcoming the limitations of traditional imaging modalities. These advancements are pivotal for the progression of personalized medicine, ensuring targeted and effective treatments.

2D MoS_2 in combination therapy

The need for increased antitumor efficacy has led to a gradual shift from monotherapy to multimodal therapy. This trend further underscores the need to develop a complementary strategy aimed at achieving synergistic therapy with the desired efficacy [139]. In this context, we discuss a synergistic PTT/photodynamic therapy (PDT) strategy as an example. Importantly, drug delivery for combination therapy is not discussed here but will be addressed in the next section.

PDT is capable of generating ROS to kill cancer cells, especially in deep tissues [140]. This capacity significantly offsets the limited effectiveness of PTT in these regions. Conversely, PTT has been proven to improve tumor oxygenation, a crucial advantage in countering the tumor hypoxia commonly observed after prolonged PDT [141, 142]. Evidently, the integration of these therapies presents synergistic potential that exceeds the capabilities of each treatment. In a recent study, Qi et al. investigated the application of 2D MoS_2 in a hydrogel context [143]. This study developed an injectable polysaccharide hydrogel loaded with BSA-MoS_2 nanosheets for synergistic PTT/ PDT in breast cancer (Fig. 4D). The hydrogel enables the sustained presence of BSA-MoS_2 around tumor cells for prolonged therapeutic efficacy. Upon NIR irradiation, BSA-MoS_2 in the hydrogel demonstrates a remarkable ability to annihilate tumor cells via photothermal conversion. Additionally, under 808 nm laser irradiation, a large amount of ROS is generated within cells, augmenting the efficacy of the PDT modality in tumor management. Highlighting the synergistic impact of PTT/PDT, the weights of the tumors treated with the BSA-MoS_2 hydrogel and laser were significantly lower than those of the PBS group and even the BSA-MoS_2 with laser group (Fig. 4E-G). These findings underscore the significant potential and importance of 2D MoS_2 in multimodal treatment strategies. Such approaches could not only reduce the intensity of each treatment modality, thereby mitigating adverse reactions, but also significantly enhance the therapeutic efficacy compared with single-modality therapies. This finding supports a shift toward more personalized medical approaches.

Synergistic strategies in cancer-targeting drug delivery

The high specific surface area of 2D MoS_2 makes it an excellent drug carrier. Through surface modification, the hydrophilicity, stability, and biocompatibility of 2D MoS_2 can be improved, making it an ideal delivery platform that provides an effective solution for drug insolubility and the degradation of genes and immune reagents [38, 144, 145]. Effective cancer treatment relies not only on the design of therapeutic agents but also on their ability to reach and penetrate tumor tissues efficiently. In this regard, 2D MoS_2 with enhanced stability and biocompatibility allows relatively long circulation times in the bloodstream, increasing the likelihood of reaching tumor sites. The small size of 2D MoS_2 enables it to exploit the EPR effect, allowing preferential accumulation in tumor tissues due to the characteristic leaky vasculature and poor lymphatic drainage of tumors [146]. Within the TME, 2D MoS_2 can be efficiently taken up by tumor cells through endocytosis, followed by the subsequent release of drugs [147]. Moreover, 2D MoS_2 conjugated with targeting ligands can achieve increased tumor specificity and reduce off-target effects [148]. The transport oncophysics of 2D MoS_2 is still insufficiently described. Issues such as the fluid dynamics of 2D MoS_2 and methods to overcome the extracellular matrix barrier

Table 1 Functionalized 2D MoS_2 for drug delivery and theranostic

Platform	Biocompatibility modification	Targeted modification	Loaded agent	Applications	Year	Refs.
MoS2-PEG-RGD-SPDP-DOX	PEG	RGD	DOX	Chemotherapy, PTT	2022	[78]
CpG@MM-PL			CpG	Immunotherapy	2023	[145]
MoS_2-RBC-DOX	RBC membrane	RBC membrane	DOX	Chemotherapy, PTT	2022	[156]
MoS_2@BT-PDA-FA-Gem	BT, PDA	FA	Gem	Chemotherapy, PTT	2023	[157]
DOX-Biotin-BSA-PEI-LA-MoS_2-LA-PEG	PEG, BSA	Biotin	DOX	Chemotherapy, PTT	2022	[147]
MoS_2-PEG-Biotin-Cur/Er	PEG	Biotin	Cur, Er	Chemotherapy, PTT	2023	[160]
HAPM@siPDL1		HA	siPDL1	Gene therapy, mild PTT	2024	[173]
MoS_2-aPDL1-V9302			aPDL1, V9302	Immunotherapy, targeted therapy	2022	[187]
Cy7.5-TG@GPM	HPG	Glucose	Cy7.5	PDT	2022	[190]
MoS_2-TFPy			TFPy	PTT, PDT	2024	[191]
IL-MoS_2-PEG-b-PIL@DOX	PEG-b-PIL		DOX	Chemotherapy, PTT, PAI	2023	[194]
MoS_2-PEG	PEG			PTT, PCT, PAI, thermal imaging	2023	[195]
MoS_2-PEG-TOS-FA	PEG	FA	TOS	Chemotherapy, PTT, CT, PAI, thermal imaging	2021	[196]
1-MT-Pt-PPDA@MoS_2	PEG, PDA		1-MT, Pt	Immunotherapy, chemotherapy, PTT, CT, PAI	2021	[199]
GA/MoS_2/BSA-Gd_2O_3-HA	BSA	HA	GA, Gd_2O_3	Chemotherapy, low-temperature PTT, MRI	2021	[204]

Molybdenum disulfide (MoS_2), polyethylene-glycol (PEG), arginine-glycine-aspartate (RGD), succinimidyl 3-[2-pyridyldithio] propionate (SPDP), doxorubicin (DOX), cytosine-phosphate-guanine (CpG), medium-sized MoS_2 (MM), low PEI0.8 k coverage (PL), erythrocyte (RBC), barium titanate (BT), polydopamine (PDA), folic acid (FA), gemcitabine (Gem), bovine serum albumin (BSA), polyethylenimine (PEI), lipoic acid (LA), curcumin (Cur), erlotinib (Er), hyaluronic acid (HA), 6-azidohexylguanidine-rich α-helical polypeptide-decorated amino-modified MoS_2 (APM), programmed death-ligand 1 (PD-L1), PD-L1 siRNA (siPDL1), anti-PDL1 antibody (aPDL1), hyperbranched polyglycidyl (HPG), triphenylphosphonium-glibenclamide (TG), glucose-HPG functionalized MoS_2 (GPM), 5-(4-(diphenylamino) phenyl) furan-2-pyridine (TFPy), ionic liquid (IL), α-tocopheryl succinate (α-TOS), 1-methyl-tryptophan (1-MT), cisplatin (Pt), gambogic acid (GA), cadmium trioxide (Gd_2O_3), photothermal therapy (PTT), photodynamic therapy (PDT), photoacoustic imaging (PAI), piezo-catalytic therapy (PCT), computerized tomography (CT), magnetic resonance imaging (MRI)

require further investigation to improve drug delivery efficiency [149, 150]. Undeniably, 2D MoS_2 has shown promising potential in cancer-targeting drug delivery. In the following paragraphs, we discuss the progress in drug delivery-based combination therapies (Table 1).

Chemotherapy-based combination therapy

The atomically thin planar structure and extraordinary surface-area-to-volume ratio of 2D MoS_2 makes it an ideal drug carrier for drug delivery applications [38]. In addition, its combination with antitumor agents, such as doxorubicin (DOX), further endows 2D MoS_2 with the ability to treat different malignancies [151]. In view of the photothermal effects and chemotherapeutic potential conferred by drug loading, the combination of these two modalities is anticipated to generate superior therapeutic outcomes.

In a pioneering work, Liu et al. documented the tremendous potential of 2D MoS_2 in drug delivery and cancer combination therapy [79]. Specifically, drug loading ratios of up to ~ 239% for DOX were achieved by electrostatic attraction. This performance is a substantial advancement considering the typical range of 10–30% observed in conventional nanoparticle-based drug delivery systems. Following PEG modification, the resulting MoS_2-PEG-DOX nanosheets exhibited enhanced biocompatibility, leading to a safer antitumor response. However, single injections of MoS_2-PEG-DOX did not yield satisfactory therapeutic outcomes, as evidenced by slightly delayed tumor growth in the absence of NIR laser irradiation. In sharp contrast, the combination of chemotherapy and PTT with MoS_2-PEG/DOX and NIR irradiation led to the dramatic inhibition of tumor growth [19].

Although MoS_2-PEG has shown high biocompatibility and efficacy in chemo-photothermal therapy, the linear polymers represented by PEG could be subject to more rapid clearance from the blood circulation than their branched counterparts, potentially leading to inadequate treatment durability [152]. Wang et al. developed branched hyperbranched polyglycidyl (HPG)-modified MoS_2 (MoS_2-HPG) by absorbing HPG onto the surface of MoS_2 to address this issue, and this molecule displayed excellent dispersion, stability, biocompatibility, and, most importantly, a prolonged in vivo circulation time. Additionally, MoS_2-HPG was utilized as a drug carrier

to deliver DOX, producing superior antitumor effects through chemo-photothermal therapy [153]. Based on these findings, MoS_2-HPG was further employed for the codelivery of DOX and chloroquine (CQ). Importantly, MoS_2-HPG exhibited a high degree of loading efficiency for DOX and CQ, with rates of 88.9% and 92.4%, respectively. Furthermore, the release of drugs from the nanosheets was significantly enhanced by laser irradiation, resulting in the efficient eradication of incubated multidrug-resistant HeLa cells [154]. Nonetheless, exogenous substances can ultimately be eliminated by the immune system, underscoring the need for endogenous materials such as erythrocyte (RBC) membranes to prolong the retention time in the blood and enhance therapeutic efficacy [155]. Li et al. designed an RBC membrane-camouflaged MoS_2-based nanosystem for DOX delivery to address this issue [156]. In this system, the RBC membrane contributes to the synergistic effect of chemotherapy and PTT by MoS_2-DOX, enabling the nanoparticles to effectively enter tumor tissue with enhanced hydrophilicity, immune evasion capability and long circulation properties.

Tumor-specific ligands such as FA, peptides and biotin were incorporated onto the surface of 2D MoS_2 to further improve the therapeutic efficacy and minimize unwanted effects. Murugan et al. constructed an FA-based targeting core–shell nanoparticle, MoS_2@ barium titanate (BT)-PDA-FA (MBPF), with BT and PDA providing excellent biocompatibility [157]. This platform was then adapted to carry gemcitabine (Gem), amalgamating chemotherapy with PTT. Through FA receptor-mediated endocytosis, MBPF was internalized, and Gem was released into the cytoplasm. Upon exposure to the NIR laser, heat was generated, simultaneously promoting Gem release and increasing the therapeutic effect. In addition, compared with Gem-loaded MBPF (34.6%), MBPF + NIR (39.8%), and MoS_2@BT (31.8%), breast cancer cells exposed to MBPF + Gem + NIR exhibited increased cytotoxicity (81.3%). In addition, Mo et al. chemically attached the αvβ3 integrin binding peptide RGD to MoS_2-PEG [78]. They further combined it with thiolated DOX (SH-DOX) via a disulfide linkage, leading to the creation of the RGD/MoS_2/DOX nanodrug system, termed MoS_2-PEG-RGD-succinimidyl 3-[2-pyridyldithio] propionate (SPDP)-DOX (MPRS-DOX) (Fig. 5A). This innovative methodology endows MoS_2 with the ability to target αvβ3 integrin and respond to GSH, resulting in an increase in antitumor efficiency (Fig. 5B, C). In vitro experiments revealed that HeLa cells overexpressing αvβ3 integrin exhibited a viability rate of approximately 67% when treated with the MPRS-DOX nanodrug containing 1.25 μg/mL DOX for 48 h. This percentage was notably less than the 98% viability observed in cells treated with MPRS alone. Moreover, when the dose of the MPRS-DOX nanodrug was increased to 10 μg/mL DOX, the viability of the HeLa cells decreased to 22.2%. Impressively, when αvβ3 integrin was combined with 808-nm NIR laser irradiation, the cytotoxic impact on αvβ3 integrin-overexpressing tumor cells intensified, reducing HeLa cell viability to 45% (Fig. 5D).

Similarly, a MoS_2-based biotin-functionalized nanoplatform was developed for targeted delivery. Due to the heightened demand for biotin for the accelerated growth of cancer cells, biotin receptors (BiRs) are overexpressed in cancer cells, making them important targets for cancer diagnosis and treatment [158, 159]. In light of this information, Liu et al. developed an innovative MoS_2-based nanoplatform, DOX-Biotin-BSA-polyethyleneimine (PEI)-lipoic acid (LA)-MoS_2-LA-PEG (DOX-BBPL-MoS_2-LP), which was enhanced with LA-PEG and BSA to increase its dispersibility and colloidal stability and incorporated biotin to enable the specific targeting of human cervical cancer cells [147]. The engineered nanoplatform generates considerable heat upon NIR light (808 nm) stimulation, not only ablating tumors but also facilitating the targeted release of DOX. This process enables potent synergy between PTT and chemotherapy. In addition, Chen et al. utilized a biotin-enhanced nanodrug delivery system to achieve the codelivery of curcumin (Cur) and erlotinib (Er) [160]. Cur is known to inhibit Er resistance by maintaining Ikappa-B expression and reducing phosphatidylinositol kinase levels in the epidermal growth factor receptor downstream signaling pathway [161, 162]. This action facilitates the release of the apoptotic proteins caspase-3 and caspase-9, thereby promoting the apoptosis of tumor cells and enhancing the effectiveness of chemotherapy [163]. Upon NIR irradiation, MoS_2-PEG-Biotin efficiently converts the absorbed light into heat, enabling the photothermal ablation of cancer cells and consequently enhancing the antitumor efficacy. Research indicates that MoS_2-PEG-Biotin-Cur/Er has a remarkable tumor growth inhibition rate of approximately 95.6% and significantly reduces the tumor volume under NIR irradiation, which is attributed mainly to the dynamic combination of enhanced synergistic chemotherapy and PTT [160]. Notably, 2D MoS_2 has been extensively investigated as a carrier for chemotherapeutic drug delivery. The innovative approaches discussed, including high drug loading capacities, enhancements in biocompatibility, and novel delivery strategies, underscore the potential of 2D MoS_2 to serve as an exemplary carrier. The integration of 2D MoS_2 with various functional modifications demonstrates its versatility as a platform for enhancing the efficacy and safety of chemotherapy and PTT.

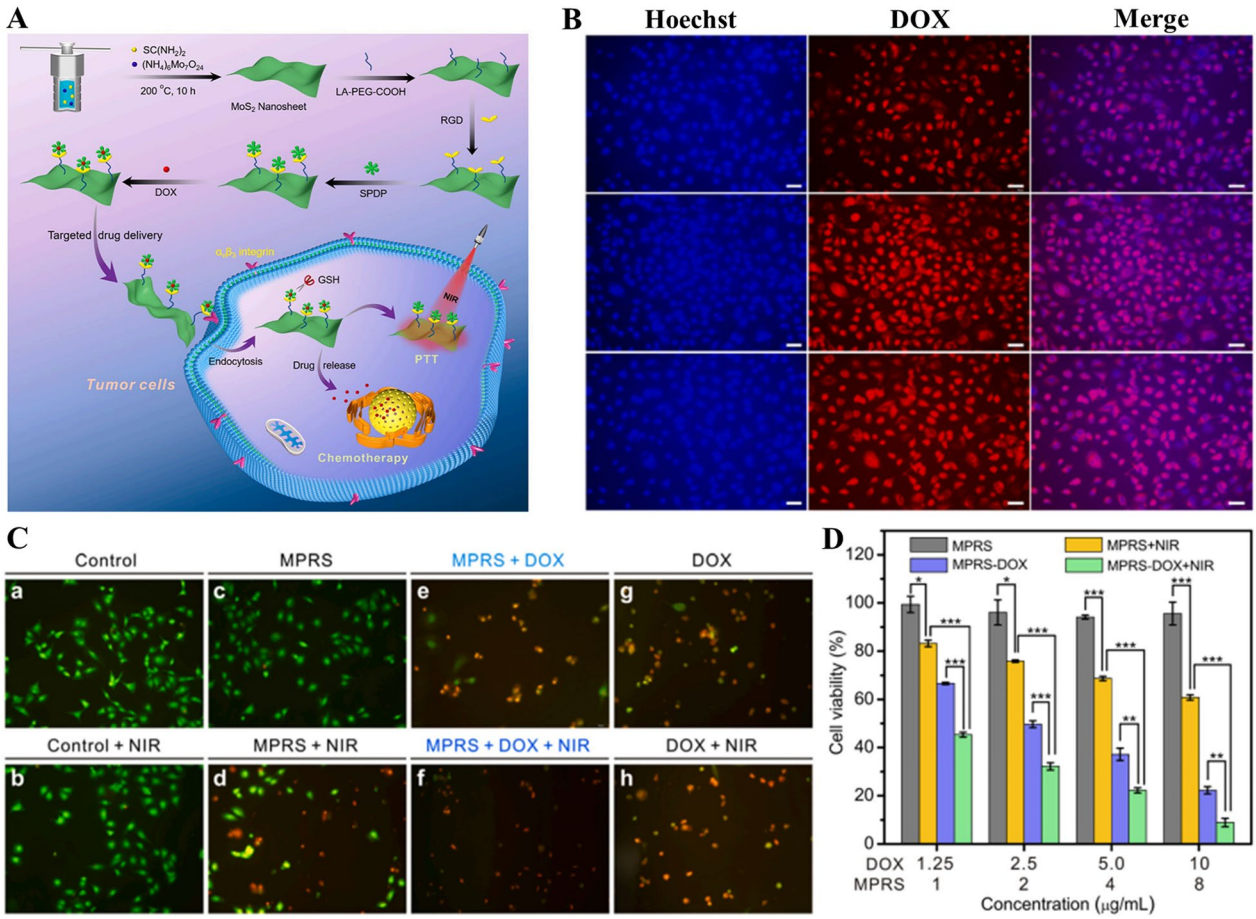

Fig. 5 **A** Schematic diagram of MoS_2/RGD/DOX nanodrug preparation for targeted delivery, intracellular GSH-triggered DOX release, and synergistic chemo/photothermal antitumor therapy. **B** Fluorescence microscope images showing the uptake of MPRS-DOX by Hela cells. **C** Fluorescence microscope images showing Hela cells apoptosis in different treatment groups. **D** Cell viability of Hela cells under different treatments. Reproduced with permission [78]. Copyright 2022, Elsevier

Gene therapy-based combination therapy

Small interfering RNA (siRNA)-induced gene therapy has been identified as a promising and innovative approach for cancer treatment, as it can effectively inhibit tumor development by suppressing the expression of specific genes [164, 165]. Nonetheless, the naked form of siRNA is susceptible to degradation by both intracellular and extracellular nucleases, while its negatively charged nature hinders its cellular uptake [166]. The key to successful gene therapy relies heavily on the development of suitable siRNA carriers for efficient siRNA delivery into cells. In this context, the potential use of 2D MoS_2 in siRNA delivery has been explored, given its exceptional ability to deliver chemotherapeutic agents.

Polo-like kinase 1 (PLK1), a well-known oncogene, is a critical regulator of DNA replication [167]. Kou et al. synthesized MoS_2-PEG-PEI, wherein PEI provided a positive charge to bind to and deliver the negatively charged PLK1 siRNA [168]. Following MoS_2-induced siRNA transfection, the efficacy of PLK1 silencing achieved with MoS_2-PEG-PEI/siPLK1 was comparable to that achieved with Lipofectamine 2000 at an N/P ratio of 20. Notably, as the N/P ratio increased, the proportion of apoptotic cells treated with MoS_2-PEG-PEI/siPLK1 increased, indicating the efficacy of MoS_2 as a transfection carrier and the promise of gene therapy. In addition, the synergy of PTT and gene therapy is expected to yield more favorable outcomes. Kong et al. constructed a generation 5 (G5) poly(amidoamine) dendrimer-MoS_2 (G5-MoS_2) platform for the combination B-cell lymphoma-2 (Bcl-2) gene silencing and PTT of tumors (Fig. 6A) [169]. The G5 dendrimers possess both a compact size and positive surface potential. These characteristics are pivotal, as they aid in the delivery of the Bcl-2 siRNA, enabling the downregulation of the Bcl-2 protein in cancer cells and inhibiting their growth. On the other hand, under photothermal conditions, the destruction of cancer cell

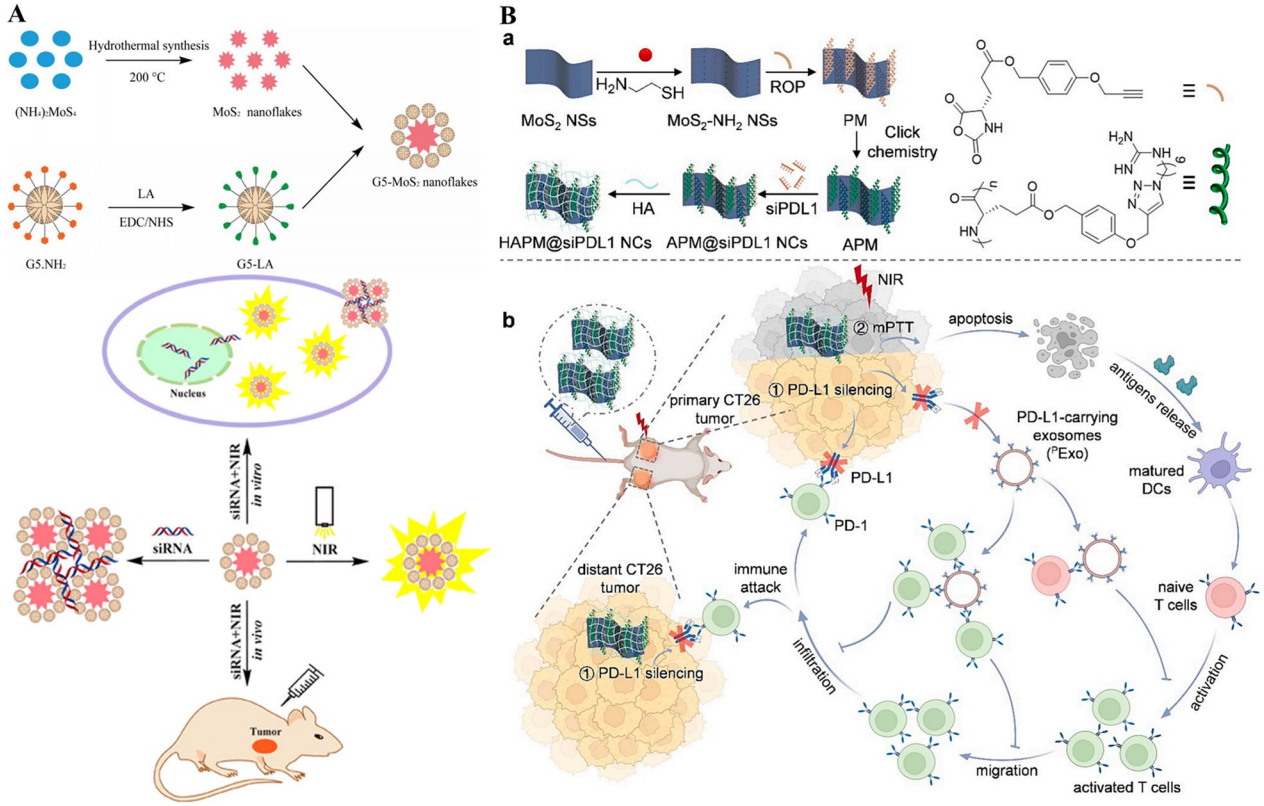

Fig. 6 **A** Schematic diagram of the synthesis of G5-MoS_2 nanosheets and combinational gene silencing and PTT. **B** Schematic illustration of preparation of HAPM@siPDL1 and HAPM@siPDL1-mediated PD-L1 down-regulation and mPTT. Reproduced with permission [169]. Copyright 2017, American Chemical Society. Reproduced with permission [173]. Copyright 2024, Elsevier

skeletons through hyperthermia-induced mechanisms can be achieved, resulting in synergistic cancer cell therapy [169, 170]. The evidence of its effectiveness is clear: a marked decrease in cell viability was observed when cells were treated with G5-MoS_2/siRNA polyplexes and laser irradiation, in contrast to cells treated with standalone siRNA with or without laser treatment. In support of these findings, in vivo experiments revealed that while G5-MoS_2/siRNA treatment inhibited tumor growth to some extent, coupling G5-MoS_2/siRNA treatment with laser irradiation not only considerably suppressed growth but also achieved complete tumor elimination. This finding underscores the strong synergy between PTT and gene silencing [169].

Instead of directly inhibiting or eliminating tumors, as with traditional oncogenes, innovative platforms are being developed to silence immune checkpoint-related genes to enhance antitumor immune responses. Programmed cell death protein 1/programmed death-ligand 1 (PD-1/PD-L1) is a classic immune checkpoint that enables tumor cells to foster an immunosuppressive TME through the overexpression of PD-L1 [171, 172]. In light of these findings, Ye et al. developed a nanoplatform that carries PD-L1 siRNA (siPDL1), resulting in potent antitumor immune reactions [173]. A 6-azidohexyl guanidine-rich α-helical polypeptide and HA were combined with 2D MoS_2 to form HAPM@siPDL1 through complexation with siPDL1 to construct the nanoplatform (Fig. 6B). After targeted accumulation in tumors, HAPM@siPDL1 provoked efficient cytosolic delivery and PD-L1 silencing due to the potent membrane-penetrating capability of the polypeptides, resulting in attenuated immunosuppression. Importantly, the combination with mild PTT, characterized by tumor cell ablation in the low-temperature range (42–46 °C), complements this effect by enhancing immunogenicity through tumor cell apoptosis and antigen release [174]. This synergistic action with siPD-L1 maximized the antitumor immune response, effectively increasing immunosuppression and reinstating immune surveillance. It has also displayed remarkable antitumor efficacy, with an approximately 95% tumor inhibition rate observed in mice treated with HAPM@siPDL1 under NIR irradiation within the 18-day observation period [173]. From delivering siRNAs that target oncogenes such as PLK1 to engaging immune checkpoints such as PD-L1,

2D MoS_2 has versatile potential for both direct cancer treatment and immunomodulation. Building on this foundation, the integration of gene silencing with PTT represents a more effective approach to cancer therapy. Future research should not be confined to siRNAs alone; broader gene therapy strategies, including the use of messenger RNA and antisense oligonucleotides, should be explored to broaden the therapeutic potential [175].

Immunotherapy-based combination therapy

In recent years, immunotherapy has emerged as a powerful clinical strategy for cancer treatment. By employing the immune system to eradicate cancer cells, immunotherapy has demonstrated robust antitumor activity while mitigating metastasis and recurrence [176]. Various agents, such as cytosine–phosphate–guanine (CpG) and anti-PDL1 antibodies (aPDL1), are often used to augment the activation of the immune system against cancer cells [177, 178]. Importantly, combination with delivery nanoplatforms could further increase cancer immunotherapy efficiency and reduce off-target adverse effects by increasing the accumulation within tumor tissues and the internalization of immunotherapeutic components [179].

Currently, 2D MoS_2 is being investigated as a vehicle for immunoreagents. For example, Han et al. fabricated MoS_2-PEG-CpG to deliver the immune adjuvant CpG for photothermal-enhanced immunotherapy [180]. The mammalian immune system recognizes CpG through Toll-like receptor 9. This interaction leads to the release of anticancer cytokines, activates helper T-cell 1-based cellular and humoral effector functions, and subsequently induces potent cytotoxic T lymphocyte (CTL) activity [177, 181, 182]. However, these nucleic acids cannot easily cross the cell membrane due to their negative charges, and they are vulnerable to degradation by nucleases [183, 184]. Therefore, the delivery of CpG via MoS_2 represents a highly desirable solution to this challenge. Importantly, 2D MoS_2 loaded with CpG has been applied to target head and neck squamous cell carcinoma, a cancer type characterized by a highly immunosuppressive TME [185, 186]. Li et al. coated medium-sized and CpG-loaded 2D MoS_2 with low $PEI_{0.8\ k}$ coverage to synthesize CpG@MM-PLs (Fig. 7A) [145]. CpG@MM-PLs effectively promoted dendritic cell (DC) maturation and CTL function, thereby potentially reversing immunosuppression in this challenging context. In vivo, CpG@MM-PL treatment effectively

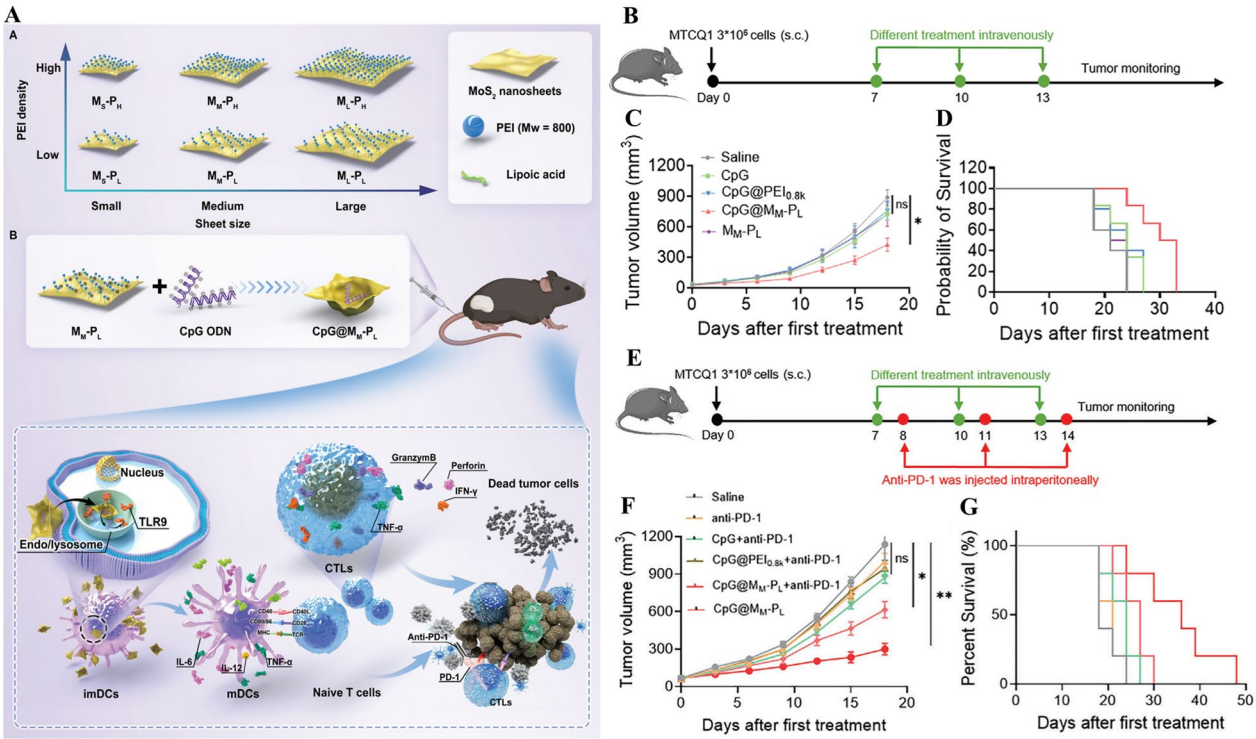

Fig. 7 **A** Schematic diagram of CpG@MM-PL preparation and its antitumor therapy. **B** Schematic diagram and timeline of antitumor treatment with CpG@MM-PL. Tumor growth (**C**), survival curves (**D**) of mice with different treatments. **E** Schematic diagram and timeline of antitumor treatment with CpG@MM-PL combined with PD-1 antibody. Tumor growth (**F**), survival curves (**G**) of mice with different treatments. Reproduced with permission [145]. Copyright 2023, Wiley

reduced tumor growth (Fig. 7B-D). Notably, when combined with immune checkpoint blockade, CpG@MM-PLs exhibited an increased capacity to retard tumor growth, which was significantly greater than that of single CpG@MM-PL treatment (Fig. 7E-G).

In addition to mere combination therapies, the codelivery of immune enhancers and checkpoint inhibitors has been successfully implemented. Tang et al. pioneered a codelivery platform, MoS_2-aPDL1-V9302, designed for delivering both aPDL1 and V9302, aiming to amplify the anticancer immune response in triple-negative breast cancer cells [187]. The glutamine transporter inhibitor V9302 selectively targets alanine–serine–cysteine transporter 2, effectively obstructing glutamine absorption and thus reversing the nutritional deprivation exerted by cancer cells on immune cells [188]. Importantly, V9302 prompts the strategic repositioning of tumor-infiltrating lymphocytes from the periphery of the tumor to its core [189]. This shift creates a conducive environment for immune checkpoint inhibitors to function, specifically by blocking additional PD-L1. The resulting synergy between V9302 and aPDL1 is evident in their ability to significantly increase lymphocyte proliferation, enhance lymphocyte functionality, and increase the effectiveness of anti-PDL1 therapy. In vivo experiments have shown that the administration of MoS_2-aPDL1-V9302 leads to elevated glutamine levels in the tumor interstitial fluid, which correlates with a substantial increase in activated CTLs, effectively inhibiting the growth of tumors [187]. In conclusion, by facilitating the delivery of immune adjuvants such as CpG and aPDL1, 2D MoS_2 nanoplatforms address significant challenges such as immune suppression within the TME. The use of 2D MoS_2 not only improves the stability and efficacy of the immunoreagents but also synergistically enhances their therapeutic outcomes, particularly when combined with other treatments such as PTT and checkpoint inhibitors, demonstrating promising capabilities in advancing cancer immunotherapy.

Photodynamic therapy-based combination therapy

2D MoS_2 has been leveraged not only for its role in catalyzing the generation of ROS for PDT but also as a carrier for agents to increase PDT efficiency. Xu et al. employed glucose-HPG-functionalized MoS_2 (GPM) for the targeted delivery of the PDT dyes triphenylphosphonium (T) and glibenclamide (G) conjugated with Cy7.5 (Cy7.5-TG@GPM) (Fig. 8A) [190]. This formulation achieves dual tumor- and subcellular-targeted PDT. Specifically, Cy7.5-TG@GPM can target tumor cells expressing high levels of glucose transporter 1, ensuring significant tumor uptake. Upon exposure to NIR, Cy7.5-T and Cy7.5-G are released, which target the mitochondria and ER, respectively. This release triggers the production of ROS that impair mitochondria and provoke ER stress, leading to the death of tumor cells. In detail, ROS-induced ER stress not only initiates the proapoptotic signaling cascade but also cooperatively promotes the release of cytochrome C from the mitochondria, causing tumor cell apoptosis. Moreover, such mitochondrial dysfunction disrupts ATP production, which in turn downregulates the expression of multidrug resistance (MDR)-related P-glycoprotein, thus contributing to overcoming MDR. The in vivo studies revealed remarkable success in inhibiting tumor growth and reversing MDR in multidrug-resistant HeLa cell tumors in nude mice, highlighting its potential for advanced therapeutic strategies (Fig. 8B).

In addition to the potent outcomes of 2D MoS_2 in PDT, further investigations have focused on the synergistic application of PDT and PTT to achieve better efficacy. In a pioneering work, Li et al. synthesized a novel nanocomposite, MoS_2-TFPy, by intercalating aggregation-induced emission luminogens (AIEgens) mercapto-PEG-5-(4-(diphenylamino) phenyl) furan-2-pyridine (TFPy-SH) into the layers of MoS_2 nanosheets (Fig. 8C) [191]. This process not only expanded the interlayer spacing of the MoS_2 nanosheets but also induced a crystal phase transformation from 2H to 1 T. As a consequence of this structural transformation, compared with the pristine material, MoS_2-TFPy demonstrated an enhanced capability for photothermal conversion. The incorporation of positively charged AIEgens granted MoS_2-TFPy the ability to accurately target mitochondria and increase the efficiency of ROS generation, establishing it as a highly effective photosensitizer in PDT applications. The therapeutic platform built on MoS_2-TFPy integrated the enhanced PTT effect of MoS_2-TFPy with the PDT efficacy of TFPy-SH, culminating in a synergistic '1 + 1 > 2' effect on tumor therapy. Comparative in vitro and in vivo studies revealed that the antitumor efficacy of individual PTT (MoS_2 + NIR) or PDT (MoS_2 + white light) treatments and simple combinations of PTT and PDT (MoS_2 + TFPy-SH + white light + NIR) were significantly inferior to that of the combined MoS_2-TFPy + white light + NIR treatment, thereby underscoring the superior synergistic antitumor effect (Fig. 8D, E). These studies highlight the significant potential of 2D MoS_2 in PDT and its combination with PTT for enhanced cancer treatment. By serving as a carrier for PDT agents and facilitating their targeted delivery to tumor cells, 2D MoS_2 not only improves the efficiency of ROS generation but also enhances subcellular targeting, contributing to the comprehensive eradication of cancer cells.

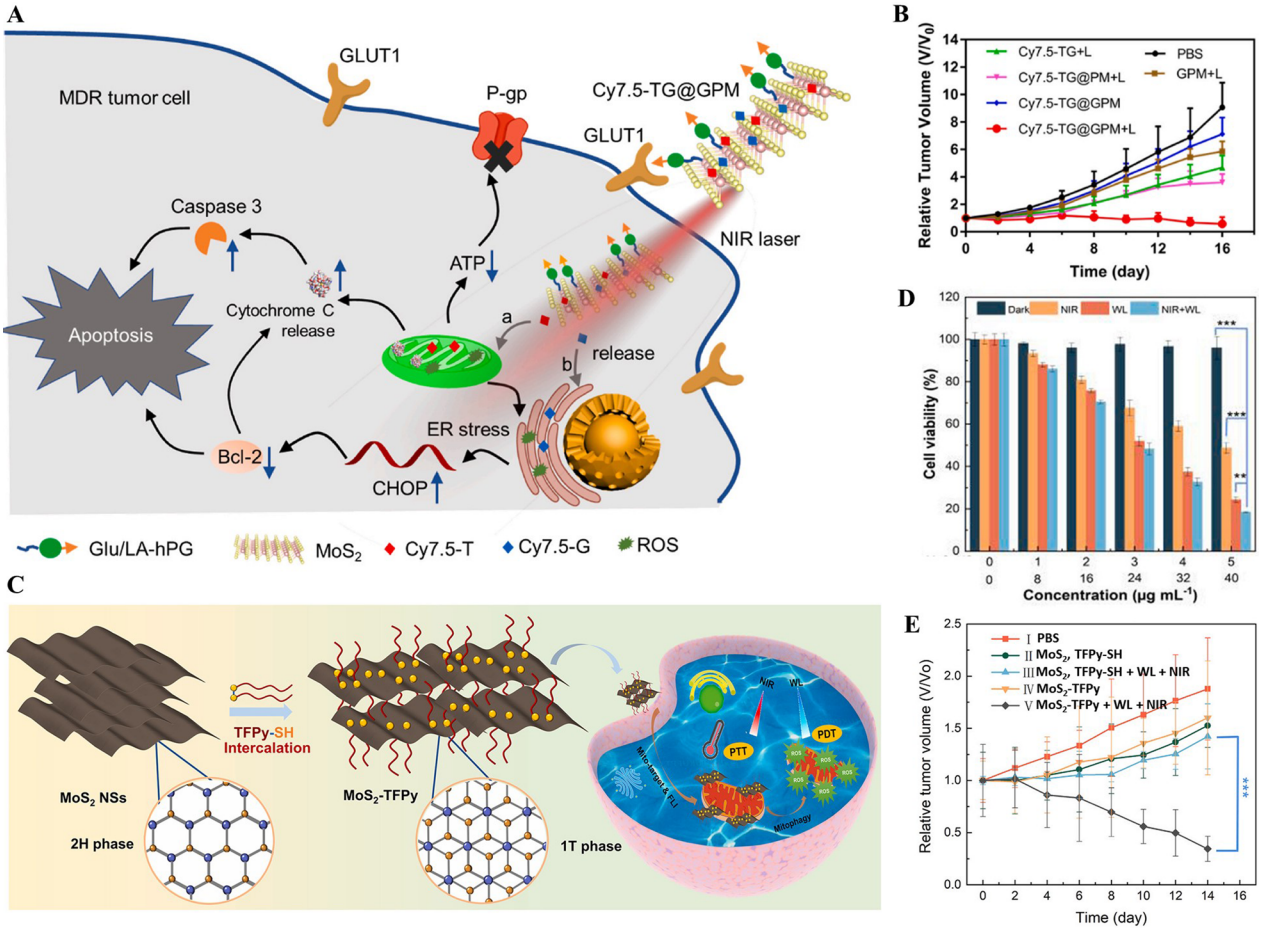

Fig. 8 **A** Schematic illustration of mitochondria and ER-targeting synergistic PDT by Cy7.5-TG@GPM under NIR irradiation. **B** Relative tumor volume of mice under different treatments. **C** Schematic illustration for the fabrication of MoS_2-TFPy and its synergistic anti-tumor PTT/PDT. Antitumor efficacy in vitro (**D**, relative cell viability) and in vivo (**E**, relative tumor volume) under different treatments. Reproduced with permission [190]. Copyright 2022, Elsevier. Reproduced with permission [191]. Copyright 2024, Elsevier

Furthermore, the synergistic use of MoS_2 in combined PDT and PTT treatments represents a powerful strategy to overcome drug resistance and achieve superior therapeutic outcomes.

Synergistic strategies for precision theranostic applications

The advancement of precision medicine has spurred significant interest in the development of an efficient theranostic platform that integrates imaging and therapeutic functionalities [192, 193]. In this context, 2D MoS_2 offers a promising protocol for the simultaneous application of diagnostic bioimaging and combination therapy based on PTT or drug delivery (Table 1).

The exploration of dual-mode imaging-guided combination therapy has garnered significant attention in the field of cancer treatment. This emerging approach integrates diagnostics and therapeutics, aiming to increase the precision and efficacy of cancer therapy. In a recent study, Lu et al. engineered a versatile nanoplatform, designated ionic liquid (IL)-MoS_2-PEG-block-poly(IL) (PEG-b-PIL)@DOX, for PA/thermal imaging-guided synergistic PTT/chemotherapy (Fig. 9A) [194]. This nanosheet was exfoliated with an antitumor IL and further tailored with PEG-b-PIL to improve its biodegradability, biocompatibility, and physiological stability. Its excellent photothermal properties endow it with exceptional capabilities in PAI, thermal imaging and PTT. In addition, its advantageous surface-area-to-volume ratio facilitates the efficient delivery of DOX for chemotherapy. The results revealed a pronounced PA signal at the tumor location at 12 and 24 h after intravenous administration, with the signal gradually increasing over time (Fig. 9B). Thermal imaging revealed a significant increase in temperature to 55.8 °C under 808 nm laser irradiation

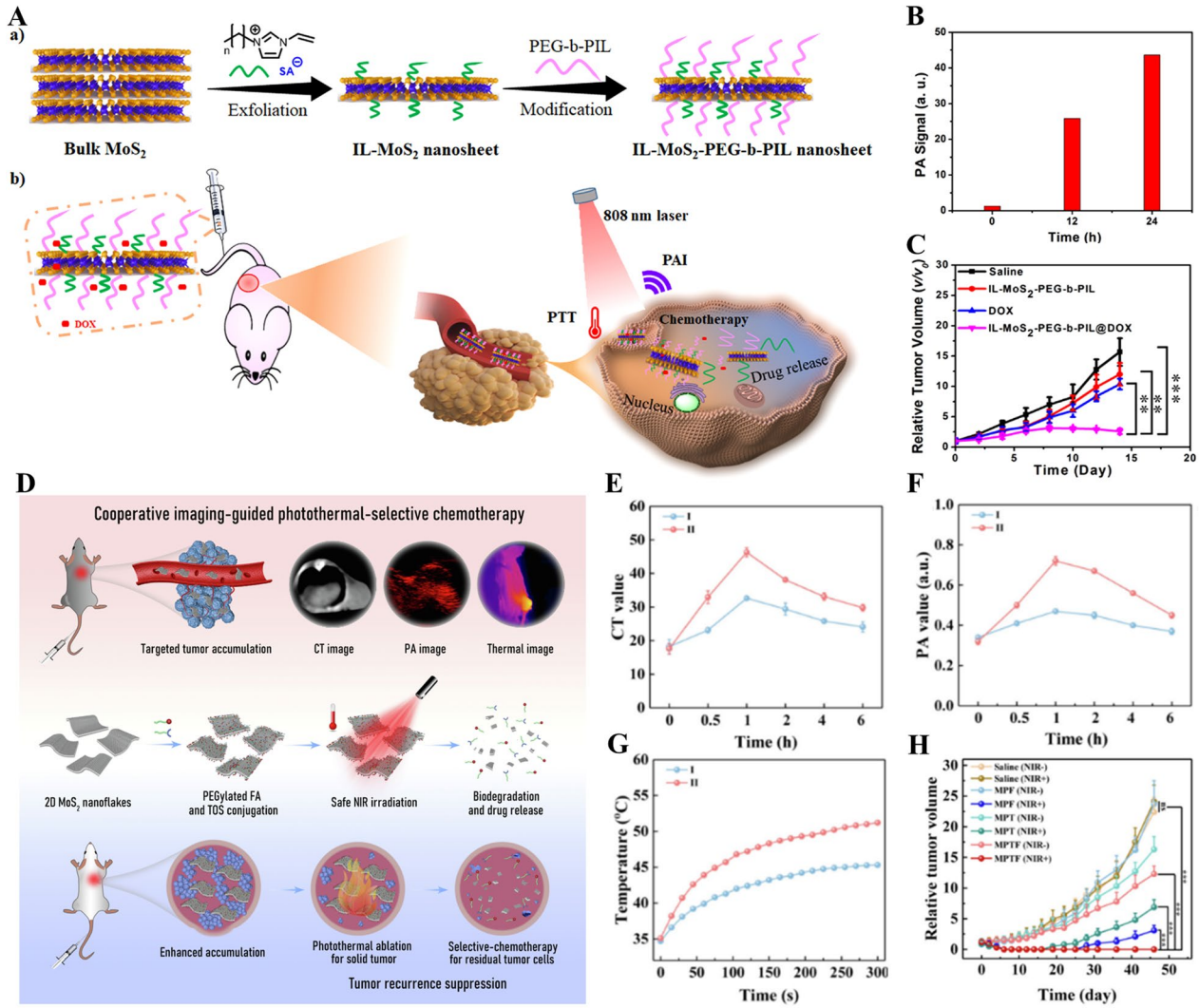

Fig. 9 **A** Schematic diagram of IL-MoS_2-PEG-b-PIL preparation and its application in synergistic photothermal/chemotherapy and PAI for cancer. **B** Quantitative analysis of PA value. **C** Relative tumor volume of mice after different treatments. **D** Schematic diagram of 2D MoS_2-based platform facilitating CT/PA/thermal imaging-guided photothermal-selective chemotherapy. CT (**E**) and PA (**F**) values of tumors in nude mice after MPT (I) and MPTF (II) intravenous injection. Thermal profiles (**G**) of tumors in nude mice under NIR irradiation after I and II intravenous injection. **H** Relative tumor volume of mice under different treatments. Reproduced with permission [194]. Copyright 2023, Wiley. Reproduced with permission [196]. Copyright 2022, Elsevier

for 10 min, which was significantly greater than that observed with the saline injection (37.1 °C). Moreover, the group treated with IL-MoS_2-PEG-b-PIL@DOX exhibited markedly superior tumor growth inhibition compared with the groups treated with IL-MoS_2-PEG-b-PIL and free DOX, underscoring the enhanced efficacy of the combination of chemo-photothermal therapy (Fig. 9C). In a parallel study, Xia et al. exploited the unique properties of MoS_2 to facilitate a PA/thermal imaging-guided combination of PTT and piezocatalytic therapy (PCT) [195]. Benefiting from the photothermal effect, MoS_2-PEG is employed not only as a potent contrast agent for PAI and thermal imaging but also as an efficacious PTA for PTT. Additionally, MoS_2-PEG exhibits a remarkable piezotronic effect, converting mechanical vibration energy into electrical energy under the stimulation of ultrasound-mediated micropressure. This conversion triggers ROS generation for cancer PCT to further kill cancer cells. After an intravenous injection of MoS_2-PEG nanosheets into 4T1 tumor-bearing mice, significant PA signals and an increase in temperature were observed under 1064 nm

laser irradiation within just 10 min. Notably, the tumors were almost completely inhibited in the experiments where the tumors were treated with MoS_2-PEG nanosheets combined with NIR and ultrasound.

Based on the promising results achieved through dual imaging, MMI-guided combination therapy has been further explored to advance the acquisition of precision medicine. In a recent study, Li et al. covalently blended PEGylated α-tocopheryl succinate (α-TOS) and FA on 2D MoS_2 to construct a comprehensive treatment platform, MoS_2-PEG-TOS-FA (MPTF) (Fig. 9D) [196]. Based on excellent CT/PA/thermal imaging capacities conferred by high atomic numbers and photothermal effects, MPTF could be employed to locate ovarian tumors preoperatively using MMI (Fig. 9E-G). The inclusion of FA ensures targeted delivery, meaning that MPTF will predominantly accumulate within tumors, paving the way for more effective treatments [197]. α-TOS can induce tumor cell apoptosis with no toxicity to healthy tissues [198]. Building on these advantages, highly efficient PTT could be activated to completely ablate the entire solid tumor under safe NIR irradiation (Fig. 9H). Finally, locally infiltrating and metastatic cancer cells are killed by α-TOS to prevent recurrence. Notably, the excellent efficacy and safety of synergistic therapy resulted in a 100% survival rate of tumor-bearing mice over 91 days [196]. Furthermore, Hu et al. developed 1-methyl-tryptophan (1-MT)-cisplatin (Pt)-PPDA@MoS_2 complexes, realizing CT/PA/thermal imaging-guided chemo-photothermal immunotherapy [199]. NIR laser irradiation (PTT) combined with Pt (chemotherapy) can destroy tumor cells and effectively induce immunogenic cell death and DC maturation, significantly bolstering T-cell-mediated antitumor immune responses. This effect is further amplified by 1-MT, which blocks the immune checkpoint associated with indoleamine 2,3-dioxygenase-mediated tryptophan metabolism. This blockade interferes with tryptophan metabolism, hindering the development of tumor-regulatory T cells and fostering the activation of T-cell-driven immunotherapy [199–201]. Impressively, the use of 1-MT-Pt-PPDA@MoS_2 with laser therapy led to complete tumor eradication in just 8 days, underscoring the unparalleled potency of this trimodal therapeutic approach. In addition, the excellent photothermal properties and X-ray absorption ability of the nanoplatform enabled comprehensive CT/PA/thermal imaging of the tumors. As expected, the CT/PAI signals of the tumors tended to increase with increasing Mo concentrations. The thermal images were also obviously obtained under 808 nm laser irradiation for 300 s, with the temperature in the tumor region increasing to 61 °C, which was much higher than that of the injection of PBS (less than 40 °C) [199].

Based on their inherent properties, loading and delivering various imaging components and therapeutic agents will lead to more possibilities in cancer therapeutics and diagnostics. For example, Liu et al. designed functionalized nanosheets termed MoS_2-HA-diethylenetriaminepentaacetic acid (DTPA)-gadolinium (Gd)/gefitinib (Gef) (Fig. 10A) [202]. These nanosheets were crafted by surface decoration with HA, conjugation with Gd ions via DTPA and the physical incorporation of Gef. The functionalized nanoplatform is capable of achieving the targeted codelivery of Gd-based contrast agents and the anticancer drug Gef, enabling both MRI and synergistic chemo-photothermal therapy. By incorporating HA as a targeting ligand, the nanosheets can efficiently direct the loaded Gd toward cancer cells that overexpress the HA receptor [203]. This targeted approach results in enhanced relaxivity, which is 3.3 times greater than that of commercial contrast agents such as DTPA-Gd, and high-resolution images of the tumor. In terms of therapy, the nanoplatform effectively converts the absorbed NIR light into heat, which not only induces the photothermal ablation of cancer cells but also spurs the release of Gef, laying the foundation for effective synergistic therapy. When measured against either chemotherapy or PTT alone, this combined approach is significantly more effective in inhibiting tumor growth in mice injected with lung cancer cells [202]. Similarly, Cai et al. revealed an integrated nanocomposite, gambogic acid (GA)/MoS_2/BSA-cadmium trioxide (Gd_2O_3)-HA (GMH), where 2D MoS_2 is functionalized with BSA-Gd_2O_3 and further augmented with GA, serving as both a chemotherapeutic and a heat shock protein 90 (HSP90) inhibitor [204, 205]. This composite is designed for MRI-guided combined low-temperature PTT (43–45 °C) and chemotherapy (Fig. 10B). BSA-Gd_2O_3, an MRI contrast agent, provides benefits such as excellent biocompatibility, a straightforward synthesis process, and a high relaxation rate [206]. Impressively, the T1 relaxation rate (r1) of MoS_2/BSA-Gd_2O_3 was 3.5 times higher than that of conventional Gd-DTPA. GA is particularly critical, as it specifically inhibits the overexpression of HSP90 when subjected to elevated temperatures, thereby reducing tumor thermoresistance and facilitating distinct types of apoptosis at relatively low temperatures [205]. Consequently, the integration of GA with PTT enables the killing of tumors at low temperatures without harming adjacent normal organs and effectively provides deep-seated tumors with sufficient heat to minimize recurrence. Consistent with our theoretical predictions, PTT with MoS_2/BSA-Gd_2O_3-HA resulted in only partial inhibition of tumor growth at a relatively low temperature (43 °C), whereas mice treated with GMH exhibited significant

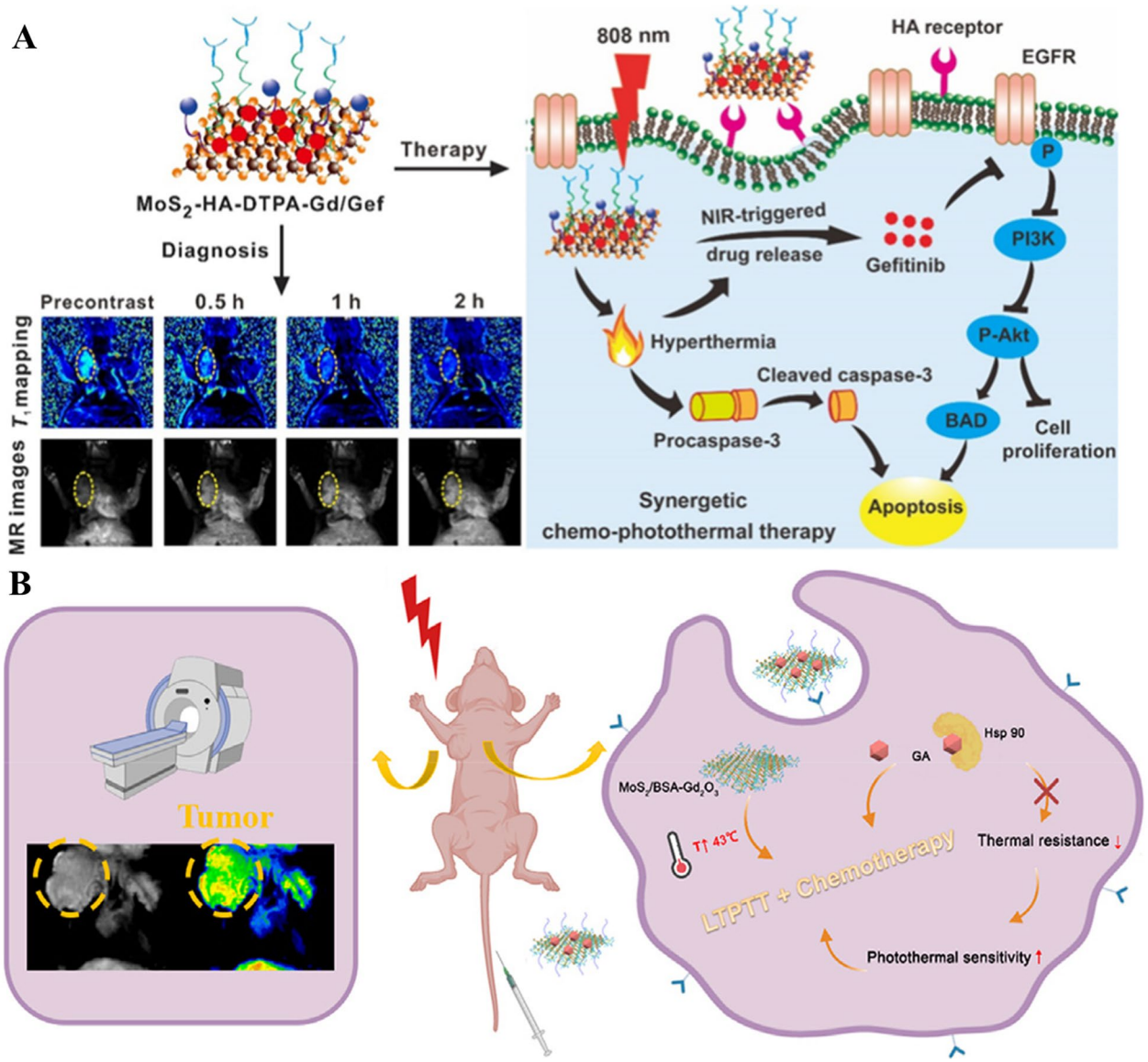

Fig. 10 **A** Schematic diagram of HA-grafted MoS_2 as a carrier for co-delivering Gef and Gd-based contrast agents for MRI guided chemo-photothermal therapy. **B** Schematic illustration of GA/MoS_2/BSA-Gd_2O_3-HA for MRI-guided combined low-temperature PTT and chemotherapy. Reproduced with permission [202]. Copyright 2019, Elsevier. Reproduced with permission [204]. Copyright 2021, Elsevier

tumor inhibition [204, 205]. The aforementioned studies illustrate the advanced utilization of MoS_2 nanoplatforms in dual-mode and MMI-guided combination therapies. These approaches represent significant progress in overcoming MDR, enhancing therapeutic efficacy, and facilitating comprehensive tumor imaging. Innovations in MoS_2-based theranostics are paving the way for more precise and effective treatments, advancing personalized medicine in oncology.

Challenges and future perspectives

The exploration of 2D MoS_2 as a theranostic platform for cancer treatment exemplifies how the primary objectives of modern oncology align with those of nanomedicine. This alignment emphasizes the development of innovative methods by integrating various treatment modalities and diagnostic techniques. This review highlights the potential of 2D MoS_2 to revolutionize cancer treatment through the development of single-mode theranostic and synergistic platforms that combine

diagnostic and targeted therapeutic functionalities, aligning with the precision medicine paradigm. However, the path from the research bench to the patient bedside is laden with challenges that must be meticulously navigated.

One of the most pressing challenges is the ability to control synthesis process of 2D MoS_2 nanocomposites to ensure the uniformity, reproducibility, and scalability necessary for clinical applications [57, 207]. The complexity of the materials requires precise control over the synthesis process, which is crucial for the clinical translation of MoS_2-based theranostics. Moreover, given the unknown potential risks, evaluating the toxicity of nanomaterials is crucial. While the low toxicity of 2D MoS_2 has been preliminarily reported in cellular and murine models, the path to clinical translation requires extensive, systematic investigations [62, 65, 68]. Further assessments at both the cellular and subcellular levels are essential to fully explore the implications of these therapies, including potential side effects on organelle structure and cellular signaling pathways [208]. In murine models, toxicity is often assessed by evaluating the accumulation in organs such as the liver and lungs, as well as weight loss. However, a comprehensive assessment of biotoxicity should encompass additional systems, including the cardiovascular, reproductive, and nervous systems, to provide a holistic understanding of the potential risks [209]. Additionally, more extensive use of larger animal models and human-mimicking systems, such as organoids and microfluidic systems, is necessary to accurately represent patient biology and tumor heterogeneity [210, 211]. In conclusion, a thorough understanding of the long-term toxicity and systemic effects of these nanomaterials is essential for establishing their clinical viability.

The pursuit of increased targeting capabilities is paramount to enhance therapeutic efficacy and minimize side effects. Research on drug delivery strategies utilizing 2D MoS_2 platforms is still in its infancy. After 2D MoS_2 is successfully delivered to tumors by leveraging overexpressed receptors on tumor cell membranes and the EPR effect, utilizing both endogenous and exogenous stimuli to achieve smart regulation within tumors is crucial. Future research should focus on innovative targeting mechanisms that are responsive to biological cues such as ROS, hypoxia, and external stimuli such as ultrasound or electric fields [212]. Furthermore, the range of drugs delivered using 2D MoS_2 remains limited. Considering the rapid advancements in the application of 2D materials in drug delivery, future research on 2D MoS_2 should delve deeper into exploring its potential uses in new domains. This information is pertinent in the delivery of biologics, such as oncolytic viruses, where novel delivery mechanisms may significantly increase therapeutic efficacy [213]. Additionally, the complexity and dynamics of cancer require a deeper understanding of the antitumor effects of 2D MoS_2 nanocomposites and the exploration of potential therapeutic mechanisms.

With increasing focus on the idea of precision medicine, theranostic platforms based on 2D MoS_2 still need to be optimized. In addition to the current research into the therapeutic applications of 2D MoS_2, other treatment strategies that leverage its outstanding physicochemical properties, such as radiotherapy and sonodynamic therapy, are attracting significant interest [214]. Employing a more diversified therapeutic strategy will unlock the prospects and potential for precision medicine. For instance, Cai et al. constructed a MoS_2/BSA-Gd_2O_3 complex, where the inclusion of Gd_2O_3 enables the platform to be well suited for MRI applications [204]. Similarly, other metal elements, such as copper, can also act as functional reagents. This diverse combination of nanoparticles provides substantial scope for the development of innovative MoS_2 composites. Moreover, the heterojunction strategy should also be widely promoted within the 2D MoS_2 platform to meet the demands of precision medicine. For example, Yu et al. used a myeloid-derived suppressor cell membrane to encapsulate Fe_3O_4, thereby enhancing targeting [215]. A neutrophil membrane was used to coat black phosphorus to improve biocompatibility [216]. These strategies exemplify how similar approaches could be beneficially extended to 2D MoS_2 composites. Exploring therapeutic platforms more broadly and in greater depth should be the direction of our future research to fully harness the potential of 2D MoS_2 in medical applications.

Despite the continuously growing list of nanodrugs in patent and clinical trials, the clinical translation of 2D nanodrugs remains largely unexplored [217]. To date, few patents involving 2D MoS_2 have been reported (Table 2), and there have been no related clinical trials. This underscores the need for substantial efforts to advance this field. Achieving scalability, reducing toxicity, and optimizing therapeutic efficacy are crucial steps in the pathway to clinical translation, as mentioned above. Historically, the failure of many nanodrugs during phase II trials has been attributed predominantly to poor efficacy, suggesting that after ensuring biosafety, enhancing therapeutic efficacy is highly important [217]. Beyond the inherent challenges, the clinical translation process for 2D MoS_2 is marked by uncertainty, a common issue for 2D nanodrugs, especially for borderline products combining multiple technologies. Establishing clear regulatory guidelines for the use of 2D nanodrugs in cancer treatment is essential to ensure their successful translation through clinical trials [218, 219].

Table 2 Summary of recent patents on 2D MoS_2-based cancer theranostics

Platform	Applications	Year	Patent application number
CS-MoS_2/rGO-DOX	Chemotherapy, PTT	2023	CN117357655A
HCN@CuMS	Nanocatalytic therapy	2023	CN117427184A
MoS_2-PEG	PTT, PCT	2022	CN114569719A
MoS_2@DOX/MnO_2	Chemotherapy, PTT	2022	CN114177291A
MoS_2-RBC-DOX	Chemotherapy, PTT	2022	CN114533887A
TCPP@MoS_2-TPP	PTT, PDT	2021	CN113101366A
R837 + MoS_2@PVA	Immunotherapy, PTT	2021	CN112972680A
MoS_2-PEG-TOS-FA	Chemotherapy, PTT, CT, PAI, thermal imaging	2021	CN112957468A
1-MT-Pt-PDA@MoS_2	Immunotherapy, chemotherapy, PTT, CT, PAI	2021	CN112755185A
MoS_2-BSA-Apt	PTT, PDT	2021	CN111671901A

Molybdenum disulfide (MoS_2), polyethylene-glycol (PEG), doxorubicin (DOX), manganese dioxide (MnO_2), erythrocyte (RBC), tetra (4-carboxyphenyl) porphin (TCPP), triphenylphosphine (TPP), immune adjuvant imiquimod (R837), folic acid (PVA), α-tocopheryl succinate (α-TOS), folic acid (FA), 1-methyl-tryptophan (1-MT), cisplatin (Pt), polydopamine (PDA), bovine serum albumin (BSA), aptamer (Apt), photothermal therapy (PTT), piezo-catalytic therapy (PCT), photodynamic therapy (PDT), computerized tomography (CT), photoacoustic imaging (PAI)

The advancement of 2D MoS_2-based theranostic applications from the laboratory to clinical settings requires a concerted effort involving multidisciplinary research teams and medical practitioners. The concept of 2D MoS_2 as an "all-in-one" theranostic platform is a beacon of innovation in the field of nanomedicine, representing a significant stride toward the goal of precision medicine in cancer treatment, and it is poised to play a pivotal role in the future of oncology.

Abbreviations

2D	Two-dimensional
CT	Computerized tomography
EPR	Enhanced permeation and retention
FA	Folic acid
MRI	Magnetic resonance imaging
MoS_2	Molybdenum disulfide
NIR	Near-infrared
PEG	Polyethylene glycol
PL	Photoluminescence
PTT	Photothermal therapy
TMDs	Transition metal dichalcogenides
CVD	Chemical vapor deposition
LPE	Liquid phase exfoliation
Li	Lithium
CS	Chitosan
BSA	Bovine serum albumin
DNA	Deoxyribonucleic acid
RNA	Ribonucleic acid
ROS	Reactive oxygen species
LA	Lipoicacid
PBS	Phosphate buffered saline
RGD	Arginine-glycine-aspartate
HA	Hyaluronic acid
CD44	Cluster determinant 44
S–S	Disulfide bond
GSH	Glutathione
TME	Tumor microenvironment
PAI	Photoacoustic imaging
FI	Fluorescence imaging
PTAs	Photothermal agents
UV	Ultraviolet
MSNs	Mesoporous silica nanoparticles
H_2O_2	Hydrogen peroxide
OPD	Ortho-phenylenediamine
OH·	Hydroxyl radicals
ATP	Adenosine triphosphate
Apt	Aptamer
Ce6	Chlorine e6
Ag	Silver
DNA-AgNCs	DNA-silver nanoclusters
PA	Photoacoustic
ICG	Indocyanine green
PAA	Poly (acrylic acid)
Ab	Antibody
EMT	Epithelial-mesenchymal transition
CDs	Carbon dots
T-BTO	Tetragonal barium titanate
CA	Cinnamaldehyde
Fe	Iron
MSFP	MoS_2@SA-Fe-PEG
NH_2-PEG	Amine-polyethylene glycol
MMI	Multimodal imaging
PDA	Polydopamine
MPPF	MoS_2@PDA-PEG/peptide
NIRF	Near-infrared fluorescence
PDT	Photodynamic therapy
DOX	Doxorubicin
HPG	Hyperbranched polyglycidyl
CQ	Chloroquine
RBC	Erythrocyte
BT	Barium titanate
MBPF	MoS_2@ BT-PDA-FA
Gem	Gemcitabine
SH-DOX	Thiolated DOX
SPDP	Succinimidyl 3-[2-pyridyldithio] propionate
MoS_2-PEG-RGD-SPDP-DOX	MPRS-DOX
BiRs	Biotin receptors
PEI	Polyethylenimine
BBPL	Biotin-BSA-PEI-LA
Cur	Curcumin
Er	Erlotinib
siRNA	Small interfering RNA
PLK1	Polo-like kinase 1
G5	Generation 5

Bcl-2	B-cell lymphoma-2
PD-1	Programmed cell death protein 1
PD-L1	Programmed death-ligand 1
siPDL1	PD-L1 siRNA
CpG	Cytosine-phosphate-guanine
aPDL1	Anti-PDL1 antibody
CTL	Cytotoxic T lymphocyte
GPM	Glucose-HPG functionalized MoS_2
T	Triphenylphosphonium
G	Glibenclamide
ER	Endoplasmic reticulum
MDR	Multidrug resistance
AIEgens	Aggregation-induced emission luminogens
TFPy-SH	Mercapto-PEG-5-(4-(diphenylamino) phenyl) furan-2-pyridine
IL	Ionic liquid
PEG-b-PIL	PEG-block-poly(IL)
PCT	Piezo-catalytic therapy
α-TOS	α-Tocopheryl succinate
MPTF	MoS_2-PEG-TOS-FA
1-MT	1-Methyl-tryptophan
Pt	Cisplatin
DTPA	Diethylenetriaminepentaacetic acid
Gd	Gadolinium
Gef	Gefitinib
GA	Gambogic acid
Gd_2O_3	Cadmium trioxide
GMH	GA/MoS_2/BSA-Gd_2O_3-HA
HSP90	Heat shock protein 90
MnO_2	Manganese dioxide
TCPP	Tetra (4-carboxyphenyl) porphin
TPP	Triphenylphosphine
PVA	Folic acid

Acknowledgements
Not applicable.

Author contributions
Xinbo Yu: Writing–review & editing, Writing–original draft, Visualization, Validation, Conceptualization. Chen Xu: Writing–review & editing, Writing–original draft, Visualization, Validation, Conceptualization. Jingxu Sun: Writing–review & editing, Writing–original draft, Visualization, Validation, Funding acquisition, Conceptualization. Hainan Xu: Writing–review & editing, Writing–original draft, Visualization, Validation, Conceptualization. Hanwei Huang: Writing–review & editing, Validation. Ziyang Gan: Writing–review & editing, Validation. Antony George: Validation. Sihui Ouyang: Writing–review & editing, Writing–original draft, Visualization, Validation, Conceptualization. Funan Liu: Writing–review & editing, Writing–original draft, Visualization, Validation, Funding acquisition, Conceptualization.

Funding
This work was supported by National Key R&D Program of China [grant numbers 2019YFC1316104, 2022YFC2403401]; National Natural Science Foundation of China [Grant Numbers 81871960, 82073368, 82373110, 82102686]; and Liaoning Revitalization Talents Program [Grant Numbers XLYC2007071, XLYC1808017].

Data availability
No datasets were generated or analysed during the current study.

Declarations

Ethics approval and consent to participate
Not applicable.

Consent for publication
All authors gave their consent for publication.

Competing interests
The authors declare no competing interests.

Author details
[1]Department of Surgical Oncology and General Surgery, The First Hospital of China Medical University; Key Laboratory of Precision Diagnosis and Treatment of Gastrointestinal Tumors, China Medical University, Shenyang 110001, China. [2]Phase I Clinical Trials Center, The First Hospital of China Medical University, Shenyang 110001, China. [3]Department of Obstetrics and Gynecology, Shengjing Hospital of China Medical University, Shenyang 110004, China. [4]Institute of Physical Chemistry, Abbe Center of Photonics, Friedrich Schiller University Jena, Jena, Germany. [5]College of Materials Science and Engineering, Chongqing University, National Engineering Research Center for Magnesium Alloys, Chongqing University, Chongqing 400044, China.

Received: 21 June 2024 Accepted: 18 August 2024
Published online: 28 August 2024

References

1. Guo J, Huang L. Membrane-core nanoparticles for cancer nanomedicine. Adv Drug Deliv Rev. 2020;156:23–39.
2. Caballero D, Abreu CM, Lima AC, Neves NN, Reis RL, Kundu SC. Precision biomaterials in cancer theranostics and modelling. Biomaterials. 2022;280: 121299.
3. Fang RH, Gao W, Zhang L. Targeting drugs to tumours using cell membrane-coated nanoparticles. Nat Rev Clin Oncol. 2023;20:33–48.
4. Tagde P, Najda A, Nagpal K, Kulkarni GT, Shah M, Ullah O, Balant S, Rahman MH. Nanomedicine-based delivery strategies for breast cancer treatment and management. Int J Mol Sci. 2022;23:89.
5. Gaikwad HK, Tsvirkun D, Ben-Nun Y, Merquiol E, Popovtzer R, Blum G. Molecular imaging of cancer using X-ray computed tomography with protease targeted iodinated activity-based probes. Nano Lett. 2018;18:1582–91.
6. Sun L, Liu H, Ye Y, Lei Y, Islam R, Tan S, Tong R, Miao YB, Cai L. Smart nanoparticles for cancer therapy. Signal Transduct Target Ther. 2023;8:418.
7. Kuang F, Hui T, Chen Y, Qiu M, Gao X. Post-graphene 2D materials: structures, properties, and cancer therapy applications. Adv Healthc Mater. 2024;13: e2302604.
8. He XP, Tian H. Photoluminescence architectures for disease diagnosis: from graphene to thin-layer transition metal dichalcogenides and oxides. Small. 2016;12:144–60.
9. Decuzzi P, Pasqualini R, Arap W, Ferrari M. Intravascular delivery of particulate systems: does geometry really matter? Pharm Res. 2009;26:235–43.
10. Sethulekshmi AS, Saritha A, Joseph K, Aprem AS, Sisupal SB. MoS(2) based nanomaterials: Advanced antibacterial agents for future. J Control Release. 2022;348:158–85.
11. Zhang C, Zhang D, Liu J, Wang J, Lu Y, Zheng J, Li B, Jia L. Functionalized MoS(2)-erlotinib produces hyperthermia under NIR. J Nanobiotechnology. 2019;17:76.
12. Meng S, Zhang Y, Wang H, Wang L, Kong T, Zhang H, Meng S. Recent advances on TMDCs for medical diagnosis. Biomaterials. 2021;269: 120471.
13. Wang J, Sui L, Huang J, Miao L, Nie Y, Wang K, Yang Z, Huang Q, Gong X, Nan Y, Ai K. MoS(2)-based nanocomposites for cancer diagnosis and therapy. Bioact Mater. 2021;6:4209–42.
14. Chen F, Luo Y, Liu X, Zheng Y, Han Y, Yang D, Wu S. 2D Molybdenum sulfide-based materials for photo-excited antibacterial application. Adv Healthc Mater. 2022;11: e2200360.
15. Mphuthi N, Sikhwivhilu L, Ray SS. Functionalization of 2D MoS(2) nanosheets with various metal and metal oxide nanostructures: their properties and application in electrochemical sensors. Biosensors (Basel). 2022;12:56.
16. Huang YL, Zheng YJ, Song Z, Chi D, Wee ATS, Quek SY. The organic-2D transition metal dichalcogenide heterointerface. Chem Soc Rev. 2018;47:3241–64.
17. Wang QH, Kalantar-Zadeh K, Kis A, Coleman JN, Strano MS. Electronics and optoelectronics of two-dimensional transition metal dichalcogenides. Nat Nanotechnol. 2012;7:699–712.

18. Chou SS, Kaehr B, Kim J, Foley BM, De M, Hopkins PE, Huang J, Brinker CJ, Dravid VP. Chemically exfoliated MoS2 as near-infrared photothermal agents. Angew Chem Int Ed Engl. 2013;52:4160–4.
19. Shi J, Zhang H, Chen Z, Xu L, Zhang Z. A multi-functional nanoplatform for efficacy tumor theranostic applications. Asian J Pharm Sci. 2017;12:235–49.
20. Zhao L, Wang J, Su D, Zhang Y, Lu H, Yan X, Bai J, Gao Y, Lu G. The DNA controllable peroxidase mimetic activity of MoS(2) nanosheets for constructing a robust colorimetric biosensor. Nanoscale. 2020;12:19420–8.
21. Roy S, Deo KA, Singh KA, Lee HP, Jaiswal A, Gaharwar AK. Nano-bio interactions of 2D molybdenum disulfide. Adv Drug Deliv Rev. 2022;187: 114361.
22. Wang X, Mansukhani ND, Guiney LM, Ji Z, Chang CH, Wang M, Liao YP, Song TB, Sun B, Li R, et al. Differences in the Toxicological Potential of 2D versus aggregated molybdenum disulfide in the lung. Small. 2015;11:5079–87.
23. Kumar A, Sood A, Han SS. Molybdenum disulfide (MoS(2))-based nanostructures for tissue engineering applications: prospects and challenges. J Mater Chem B. 2022;10:2761–80.
24. Wang S, Li K, Chen Y, Chen H, Ma M, Feng J, Zhao Q, Shi J. Biocompatible PEGylated MoS2 nanosheets: controllable bottom-up synthesis and highly efficient photothermal regression of tumor. Biomaterials. 2015;39:206–17.
25. Zhang X, Wu J, Williams GR, Niu S, Qian Q, Zhu LM. Functionalized MoS(2)-nanosheets for targeted drug delivery and chemo-photothermal therapy. Colloids Surf B Biointerfaces. 2019;173:101–8.
26. Wu L, Wang C, Li Y. Iron oxide nanoparticle targeting mechanism and its application in tumor magnetic resonance imaging and therapy. Nanomedicine (Lond). 2022;17:1567–83.
27. Devasena T, Francis AP, Ramaprabhu S. Toxicity of Graphene: An Update. Rev Environ Contam Toxicol. 2021;259:51–76.
28. Zhang X, Zhang W. Synthesis of black phosphorus and its applications. Materials Today Physics. 2024;43: 101396.
29. Roy S, Zhang X, Puthirath AB, Meiyazhagan A, Bhattacharyya S, Rahman MM, Babu G, Susarla S, Saju SK, Tran MK, et al. Structure, properties and applications of two-dimensional hexagonal boron nitride. Adv Mater. 2021;33:2101589.
30. Ghosh S, Lai J-Y. An insight into the dual role of MoS2-based nanocarriers in anticancer drug delivery and therapy. Acta Biomater. 2024;179:36–60.
31. Sun J, Li X, Guo W, Zhao M, Fan X, Dong Y, Xu C, Deng J, Fu Y. Synthesis Methods of Two-Dimensional MoS2. A Brief Review. 2017;7:198.
32. Pourmadadi M, Tajiki A, Hosseini SM, Samadi A, Abdouss M, Daneshnia S, Yazdian F. A comprehensive review of synthesis, structure, properties, and functionalization of MoS2; emphasis on drug delivery, photothermal therapy, and tissue engineering applications. J Drug Deliv Sci Technol. 2022;76: 103767.
33. Wang H, Li C, Fang P, Zhang Z, Zhang JZ. Synthesis, properties, and optoelectronic applications of two-dimensional MoS(2) and MoS(2)-based heterostructures. Chem Soc Rev. 2018;47:6101–27.
34. Li H, Wu J, Yin Z, Zhang H. Preparation and applications of mechanically exfoliated single-layer and multilayer MoS_2 and WSe_2 nanosheets. Acc Chem Res. 2014;47:1067–75.
35. Grayfer ED, Kozlova MN, Fedorov VE. Colloidal 2D nanosheets of MoS(2) and other transition metal dichalcogenides through liquid-phase exfoliation. Adv Colloid Interface Sci. 2017;245:40–61.
36. Lu C, Luo M, Ge Y, Huang Y, Zhao Q, Zhou Y, Xu X. Layer-Dependent Nonlinear Optical Properties of WS(2), MoS(2), and Bi(2)S(3) Films Synthesized by Chemical Vapor Deposition. ACS Appl Mater Interfaces. 2022;14:2390–400.
37. Dong G, Li L, Zhu K, Yan J, Wang G, Cao D. Solvent Induced Activation Reaction of MoS(2) Nanosheets within Nitrogen/Sulfur-Codoped Carbon Network Boosting Sodium Ion Storage. Small. 2023;19: e2208291.
38. Yadav V, Roy S, Singh P, Khan Z, Jaiswal A. 2D MoS(2) -based nanomaterials for therapeutic, bioimaging, and biosensing applications. Small. 2019;15: e1803706.
39. Mouloua D, Kotbi A, Deokar G, Kaja K, El Marssi M, El Khakani MA, Jouiad M. Recent Progress in the Synthesis of MoS(2) Thin Films for Sensing, Photovoltaic and Plasmonic Applications: A Review. Materials (Basel). 2021;14:9.
40. Li X, Shan J, Zhang W, Su S, Yuwen L, Wang L. Recent advances in synthesis and biomedical applications of two-dimensional transition metal dichalcogenide nanosheets. Small. 2017;13:7834.
41. Li XL, Li TC, Huang S, Zhang J, Pam ME, Yang HY. Controllable synthesis of two-dimensional molybdenum disulfide (MoS(2)) for energy-storage applications. Chemsuschem. 2020;13:1379–91.
42. Joensen P, Frindt RF, Morrison SR. Single-layer MoS2. Mater Res Bull. 1986;21:457–61.
43. Chhowalla M, Shin HS, Eda G, Li LJ, Loh KP, Zhang H. The chemistry of two-dimensional layered transition metal dichalcogenide nanosheets. Nat Chem. 2013;5:263–75.
44. Yuwen L, Yu H, Yang X, Zhou J, Zhang Q, Zhang Y, Luo Z, Su S, Wang L. Rapid preparation of single-layer transition metal dichalcogenide nanosheets via ultrasonication enhanced lithium intercalation. Chem Commun (Camb). 2016;52:529–32.
45. Lin L, Miao N, Wen Y, Zhang S, Ghosez P, Sun Z, Allwood DA. Sulfur-depleted monolayered molybdenum disulfide nanocrystals for superelectrochemical hydrogen evolution reaction. ACS Nano. 2016;10:8929–37.
46. Anto Jeffery A, Nethravathi C, Rajamathi M. Two-dimensional nanosheets and layered hybrids of MoS2 and WS2 through exfoliation of ammoniated MS2 (M = Mo, W). J Phys Chem C. 2014;118:1386–96.
47. Zhang W, Wang Y, Zhang D, Yu S, Zhu W, Wang J, Zheng F, Wang S, Wang J. A one-step approach to the large-scale synthesis of functionalized MoS2 nanosheets by ionic liquid assisted grinding. Nanoscale. 2015;7:10210–7.
48. Guan G, Zhang S, Liu S, Cai Y, Low M, Teng CP, Phang IY, Cheng Y, Duei KL, Srinivasan BM, et al. Protein induces layer-by-layer exfoliation of transition metal dichalcogenides. J Am Chem Soc. 2015;137:6152–5.
49. Masoumi Z, Tayebi M, Lee BK. Ultrasonication-assisted liquid-phase exfoliation enhances photoelectrochemical performance in α-Fe(2) O(3)/MoS(2) photoanode. Ultrason Sonochem. 2021;72: 105403.
50. Xu Y, Cao H, Xue Y, Li B, Cai W. Liquid-phase exfoliation of graphene: an overview on exfoliation media, techniques, and challenges. Nanomaterials (Basel). 2018;8:89.
51. Ghasemi F, Mohajerzadeh S. Sequential solvent exchange method for controlled exfoliation of MoS(2) suitable for phototransistor fabrication. ACS Appl Mater Interfaces. 2016;8:31179–91.
52. Cunningham G, Lotya M, Cucinotta CS, Sanvito S, Bergin SD, Menzel R, Shaffer MS, Coleman JN. Solvent exfoliation of transition metal dichalcogenides: dispersibility of exfoliated nanosheets varies only weakly between compounds. ACS Nano. 2012;6:3468–80.
53. Goldie SJ, Degiacomi MT, Jiang S, Clark SJ, Erastova V, Coleman KS. Identification of graphene dispersion agents through molecular fingerprints. ACS Nano. 2022;16:16109–17.
54. Ayán-Varela M, Pérez-Vidal Ó, Paredes JI, Munuera JM, Villar-Rodil S, Díaz-González M, Fernández-Sánchez C, Silva VS, Cicuéndez M, Vila M, et al. Aqueous exfoliation of transition metal dichalcogenides assisted by DNA/RNA nucleotides: catalytically active and biocompatible nanosheets stabilized by acid-base interactions. ACS Appl Mater Interfaces. 2017;9:2835–45.
55. Seravalli L, Bosi M. A Review on Chemical Vapour Deposition of Two-Dimensional MoS(2) Flakes. Materials (Basel). 2021;14:67.
56. Ye Z, Tan C, Huang X, Ouyang Y, Yang L, Wang Z, Dong M. Emerging MoS(2) Wafer-Scale Technique for Integrated Circuits. Nanomicro Lett. 2023;15:38.
57. Liu T, Liu Z. 2D MoS(2) Nanostructures for Biomedical Applications. Adv Healthc Mater. 2018;7: e1701158.
58. Shi W, Song S, Zhang H. Hydrothermal synthetic strategies of inorganic semiconducting nanostructures. Chem Soc Rev. 2013;42:5714–43.
59. Lin H, Peng S, Guo S, Ma B, Lucherelli MA, Royer C, Ippolito S, Samorì P, Bianco A. 2D materials and primary human dendritic cells: a comparative cytotoxicity study. Small. 2022;18: e2107652.
60. García-Carpintero S, Jehová González V, Frontiñán-Rubio J, Esteban-Arranz A, Vázquez E, Durán-Prado M. Screening the micronucleus assay for reliable estimation of the genotoxicity of graphene and other 2D materials. Carbon. 2023;215: 118426.
61. Voronina MV, Frolova AS, Kolesova EP, Kuldyushev NA, Parodi A, Zamyatnin AA Jr. The Intricate Balance between Life and Death: ROS,

cathepsins, and their interplay in cell death and autophagy. Int J Mol Sci. 2024;25:8.
62. Li J, Guiney LM, Downing JR, Wang X, Chang CH, Jiang J, Liu Q, Liu X, Mei KC, Liao YP, et al. Dissolution of 2D Molybdenum Disulfide Generates Differential Toxicity among Liver Cell Types Compared to Non-Toxic 2D Boron Nitride Effects. Small. 2021;17: e2101084.
63. Wu G, Huang Y, Li J, Lu Y, Liu L, Du D, Xue Y. Chronic level of exposures to low-dosed MoS(2) nanomaterials exhibits more toxic effects in HaCaT keratinocytes. Ecotoxicol Environ Saf. 2022;242: 113848.
64. Zhao Y, Xu J, Jiang X. DNA cleavage by chemically exfoliated molybdenum disulfide nanosheets. Environ Sci Technol. 2021;55:4037–44.
65. Qiu K, Zou W, Fang Z, Wang Y, Bell S, Zhang X, Tian Z, Xu X, Ji B, Li D, et al. 2D MoS2 and BN Nanosheets Damage Mitochondria through Membrane Penetration. ACS Nano. 2023;17:4716–28.
66. Ortiz Peña N, Cherukula K, Even B, Ji DK, Razafindrakoto S, Peng S, Silva AKA, Ménard-Moyon C, Hillaireau H, Bianco A, et al. Resolution of MoS(2) nanosheets-induced pulmonary inflammation driven by nanoscale intracellular transformation and extracellular-vesicle shuttles. Adv Mater. 2023;35: e2209615.
67. D'Souza AA, Shegokar R. Polyethylene glycol (PEG): a versatile polymer for pharmaceutical applications. Expert Opin Drug Deliv. 2016;13:1257–75.
68. Hao J, Song G, Liu T, Yi X, Yang K, Cheng L, Liu Z. In vivo long-term biodistribution, excretion, and toxicology of pegylated transition-metal dichalcogenides MS(2) (M = Mo, W, Ti) Nanosheets. Adv Sci (Weinh). 2017;4:1600160.
69. Pathak R, Bhatt S, Punetha VD, Punetha M. Chitosan nanoparticles and based composites as a biocompatible vehicle for drug delivery: A review. Int J Biol Macromol. 2023;253: 127369.
70. Yin W, Yan L, Yu J, Tian G, Zhou L, Zheng X, Zhang X, Yong Y, Li J, Gu Z, Zhao Y. High-throughput synthesis of single-layer MoS2 nanosheets as a near-infrared photothermal-triggered drug delivery for effective cancer therapy. ACS Nano. 2014;8:6922–33.
71. Patel D, Solanki J, Kher MM, Azagury A. A Review: Surface Engineering of Lipid-Based Drug Delivery Systems. Small. 2024;9:e2401990.
72. Xie M, Yang N, Cheng J, Yang M, Deng T, Li Y, Feng C. Layered MoS(2) nanosheets modified by biomimetic phospholipids: Enhanced stability and its synergistic treatment of cancer with chemo-photothermal therapy. Colloids Surf B Biointerfaces. 2020;187: 110631.
73. Morales-Cruz M, Delgado Y, Castillo B, Figueroa CM, Molina AM, Torres A, Milián M, Griebenow K. Smart targeting to improve cancer therapeutics. Drug Des Devel Ther. 2019;13:3753–72.
74. Sun R, Xiang J, Zhou Q, Piao Y, Tang J, Shao S, Zhou Z, Bae YH, Shen Y. The tumor EPR effect for cancer drug delivery: Current status, limitations, and alternatives. Adv Drug Deliv Rev. 2022;191: 114614.
75. Kolate A, Baradia D, Patil S, Vhora I, Kore G, Misra A. PEG - a versatile conjugating ligand for drugs and drug delivery systems. J Control Release. 2014;192:67–81.
76. Tian H, Zhang T, Qin S, Huang Z, Zhou L, Shi J, Nice EC, Xie N, Huang C, Shen Z. Enhancing the therapeutic efficacy of nanoparticles for cancer treatment using versatile targeted strategies. J Hematol Oncol. 2022;15:132.
77. Heshmati Aghda N, Dabbaghianamiri M, Tunnell JW, Betancourt T. Design of smart nanomedicines for effective cancer treatment. Int J Pharm. 2022;621: 121791.
78. Mo C, Wang Z, Yang J, Ouyang Y, Mo Q, Li S, He P, Chen L, Li X. Rational assembly of RGD/MoS(2)/Doxorubicin nanodrug for targeted drug delivery, GSH-stimulus release and chemo-photothermal synergistic antitumor activity. J Photochem Photobiol B. 2022;233: 112487.
79. Liu T, Wang C, Gu X, Gong H, Cheng L, Shi X, Feng L, Sun B, Liu Z. Drug delivery with PEGylated MoS2 nano-sheets for combined photothermal and chemotherapy of cancer. Adv Mater. 2014;26:3433–40.
80. Dong X, Yin W, Zhang X, Zhu S, He X, Yu J, Xie J, Guo Z, Yan L, Liu X, et al. Intelligent MoS(2) Nanotheranostic for Targeted and Enzyme-/pH-/NIR-Responsive Drug Delivery To Overcome Cancer Chemotherapy Resistance Guided by PET Imaging. ACS Appl Mater Interfaces. 2018;10:4271–84.
81. Moradi Kashkooli F, Soltani M, Souri M. Controlled anti-cancer drug release through advanced nano-drug delivery systems: Static and dynamic targeting strategies. J Control Release. 2020;327:316–49.
82. Moharil P, Wan Z, Pardeshi A, Li J, Huang H, Luo Z, Rathod S, Zhang Z, Chen Y, Zhang B, et al. Engineering a folic acid-decorated ultrasmall gemcitabine nanocarrier for breast cancer therapy: Dual targeting of tumor cells and tumor-associated macrophages. Acta Pharm Sin B. 2022;12:1148–62.
83. Liu J, Li F, Zheng J, Li B, Zhang D, Jia L. Redox/NIR dual-responsive MoS(2) for synergetic chemo-photothermal therapy of cancer. J Nanobiotechnology. 2019;17:78.
84. de la Encarnación C. Multifunctional plasmonic-magnetic nanoparticles for bioimaging and hyperthermia. Adv Drug Deliv Rev. 2022;189: 114484.
85. Yang JD, Heimbach JK. New advances in the diagnosis and management of hepatocellular carcinoma. BMJ. 2020;371: m3544.
86. Steinberg I, Huland DM, Vermesh O, Frostig HE, Tummers WS, Gambhir SS. Photoacoustic clinical imaging Photoacoustics. 2019;14:77–98.
87. Zhen X, Jiang X. Polymer-based activatable optical probes for tumor fluorescence and photoacoustic imaging. Wiley Interdiscip Rev Nanomed Nanobiotechnol. 2020;12: e1593.
88. Janib SM, Moses AS, MacKay JA. Imaging and drug delivery using theranostic nanoparticles. Adv Drug Deliv Rev. 2010;62:1052–63.
89. Feng X, Lei J, Ma L, Ouyang Q, Zeng Y, Liang H, Lei C, Li G, Tan L, Liu X, Yang C. Ultrasonic Interfacial Engineering of MoS(2) -Modified Zn Single-Atom Catalysts for Efficient Osteomyelitis Sonodynamic Ion Therapy. Small. 2022;18: e2105775.
90. Luo Z, Li J, Li Y, Wu D, Zhang L, Ren X, He C, Zhang Q, Gu M, Sun X. Band Engineering Induced Conducting 2H-Phase MoS2 by PdSRe Sites Modification for Hydrogen Evolution Reaction. Adv Energy Mater. 2022;12:2103823.
91. Refaat A, Yap ML, Pietersz G, Walsh APG, Zeller J, Del Rosal B, Wang X, Peter K. In vivo fluorescence imaging: success in preclinical imaging paves the way for clinical applications. J Nanobiotechnology. 2022;20:450.
92. Li C, Chen G, Zhang Y, Wu F, Wang Q. Advanced fluorescence imaging technology in the near-infrared-II window for biomedical applications. J Am Chem Soc. 2020;142:14789–804.
93. Ma Y, Chen Q, Pan X, Zhang J. Insight into fluorescence imaging and bioorthogonal reactions in biological analysis. Top Curr Chem (Cham). 2021;379:10.
94. Qi Y, Wang N, Xu Q, Li H, Zhou P, Lu X, Zhao G. A green route to fabricate MoS2 nanosheets in water-ethanol-CO2. Chem Commun (Camb). 2015;51:6726–9.
95. Lan L, Chen D, Yao Y, Peng X, Wu J, Li Y, Ping J, Ying Y. Phase-dependent fluorescence quenching efficiency of MoS(2) nanosheets and their applications in multiplex target biosensing. ACS Appl Mater Interfaces. 2018;10:42009–17.
96. Wang J, Xu M, Wang K, Chen Z. Stable mesoporous silica nanoparticles incorporated with MoS2 and AIE for targeted fluorescence imaging and photothermal therapy of cancer cells. Colloids Surf B Biointerfaces. 2019;174:324–32.
97. Chen S, Sun X, Fu M, Liu X, Pang S, You Y, Liu X, Wang Y, Yan X, Ma X. Dual-source powered nanomotor with integrated functions for cancer photo-theranostics. Biomaterials. 2022;288: 121744.
98. Liu H, Wang B, Li D, Zeng X, Tang X, Gao Q, Cai J, Cai HH. MoS(2) nanosheets with peroxidase mimicking activity as viable dual-mode optical probes for determination and imaging of intracellular hydrogen peroxide. Mikrochim Acta. 2018;185:287.
99. Li Y, Fu R, Duan Z, Zhu C, Fan D. Adaptive hydrogels based on nanozyme with dual-enhanced triple enzyme-like activities for wound disinfection and mimicking antioxidant defense system. Adv Healthc Mater. 2022;11: e2101849.
100. Han X, Xu K, Taratula O, Farsad K. Applications of nanoparticles in biomedical imaging. Nanoscale. 2019;11:799–819.
101. Jia L, Ding L, Tian J, Bao L, Hu Y, Ju H, Yu JS. Aptamer loaded MoS2 nanoplates as nanoprobes for detection of intracellular ATP and controllable photodynamic therapy. Nanoscale. 2015;7:15953–61.
102. Xu Y, Kang Q, Yang B, Chen B, He M, Hu B. A nanoprobe based on molybdenum disulfide nanosheets and silver nanoclusters for imaging and quantification of intracellular adenosine triphosphate. Anal Chim Acta. 2020;1134:75–83.
103. He C, Zhu J, Zhang H, Qiao R, Zhang R. Photoacoustic imaging probes for theranostic applications. Biosensors (Basel). 2022;12:89.

104. Gonzalez EA, Bell MAL. Photoacoustic imaging and characterization of bone in medicine: overview, applications, and outlook. Annu Rev Biomed Eng. 2023;25:207–32.
105. Lin L, Wang LV. The emerging role of photoacoustic imaging in clinical oncology. Nat Rev Clin Oncol. 2022;19:365–84.
106. Dhas N, Kudarha R, Garkal A, Ghate V, Sharma S, Panzade P, Khot S, Chaudhari P, Singh A, Paryani M, et al. Molybdenum-based hetero-nanocomposites for cancer therapy, diagnosis and biosensing application: Current advancement and future breakthroughs. J Control Release. 2021;330:257–83.
107. Chen J, Liu C, Hu D, Wang F, Wu H, Gong X, Liu X, Song L, Sheng Z, Zheng H. Single-Layer MoS2 nanosheets with amplified photoacoustic effect for highly sensitive photoacoustic imaging of orthotopic brain tumors. Adv Func Mater. 2016;26:8715–25.
108. Teng CW, Huang V, Arguelles GR, Zhou C, Cho SS, Harmsen S, Lee JYK. Applications of indocyanine green in brain tumor surgery: review of clinical evidence and emerging technologies. Neurosurg Focus. 2021;50:E4.
109. Liu C, Chen J, Zhu Y, Gong X, Zheng R, Chen N, Chen D, Yan H, Zhang P, Zheng H, et al. Highly Sensitive MoS(2)-Indocyanine Green Hybrid for Photoacoustic Imaging of Orthotopic Brain Glioma at Deep Site. Nanomicro Lett. 2018;10:48.
110. Wu X, Suo Y, Shi H, Liu R, Wu F, Wang T, Ma L, Liu H, Cheng Z. Deep-tissue photothermal therapy using laser illumination at NIR-IIa Window. Nanomicro Lett. 2020;12:38.
111. Kumar AVP, Dubey SK, Tiwari S, Puri A, Hejmady S, Gorain B, Kesharwani P. Recent advances in nanoparticles mediated photothermal therapy induced tumor regression. Int J Pharm. 2021;606: 120848.
112. Chen L, Feng Y, Zhou X, Zhang Q, Nie W, Wang W, Zhang Y, He C. One-pot synthesis of MoS(2) nanoflakes with desirable degradability for photothermal cancer therapy. ACS Appl Mater Interfaces. 2017;9:17347–58.
113. Zhu L, Zhao J, Guo Z, Liu Y, Chen H, Chen Z, He N. Applications of Aptamer-Bound Nanomaterials in Cancer Therapy. Biosensors (Basel). 2021;11:8.
114. Pang B, Yang H, Wang L, Chen J, Jin L, Shen B. Aptamer modified MoS2 nanosheets application in targeted photothermal therapy for breast cancer. Colloids Surf, A. 2021;608: 125506.
115. Liu J, Smith S, Wang C. Photothermal attenuation of cancer cell stemness, chemoresistance, and migration using CD44-Targeted MoS(2) Nanosheets. Nano Lett. 2023;23:1989–99.
116. Xu H, Tian Y, Yuan X, Wu H, Liu Q, Pestell RG, Wu K. The role of CD44 in epithelial-mesenchymal transition and cancer development. Onco Targets Ther. 2015;8:3783–92.
117. Li Z, Ye R, Feng R, Kang Y, Zhu X, Tour JM, Fang Z. Graphene quantum dots doping of MoS2 Monolayers. Adv Mater. 2015;27:5235–40.
118. Wang J, Fu Y, Gu Z, Pan H, Zhou P, Gan Q, Yuan Y, Liu C. Multifunctional carbon dots for biomedical applications: diagnosis, therapy, and theranostic. Small. 2024;20: e2303773.
119. Geng B, Qin H, Zheng F, Shen W, Li P, Wu K, Wang X, Li X, Pan D, Shen L. Carbon dot-sensitized MoS(2) nanosheet heterojunctions as highly efficient NIR photothermal agents for complete tumor ablation at an ultralow laser exposure. Nanoscale. 2019;11:7209–20.
120. Hu R, Chen X, Li Z, Zhao G, Ding L, Chen L, Dai C, Chen Y, Zhang B. Liquid nanoparticles for nanocatalytic cancer therapy. Adv Mater. 2023;35: e2306469.
121. Kumari A, Sahoo J, De M. 2D-MoS(2)-supported copper peroxide nanodots with enhanced nanozyme activity: application in antibacterial activity. Nanoscale. 2023;15:19801–14.
122. Liu Z, Gao Y, Wen L, Wang X, Feng J, Zhu C, Li D, Zhao M. Effect of MoS2-PEG nanozymes on tumor cell multiplication. Arab J Chem. 2023;16: 105240.
123. Wang L, Zhang X, You Z, Yang Z, Guo M, Guo J, Liu H, Zhang X, Wang Z, Wang A, et al. A molybdenum disulfide nanozyme with charge-enhanced activity for ultrasound-mediated cascade-catalytic tumor ferroptosis. Angew Chem Int Ed Engl. 2023;62: e202217448.
124. Li J, Yi W, Luo Y, Yang K, He L, Xu C, Deng L, He D. GSH-depleting and H(2)O(2)-self-supplying hybrid nanozymes for intensive catalytic antibacterial therapy by photothermal-augmented co-catalysis. Acta Biomater. 2023;155:588–600.
125. Yang J, Yao H, Guo Y, Yang B, Shi J. Enhancing tumor catalytic therapy by co-catalysis. Angew Chem Int Ed Engl. 2022;61: e202200480.
126. Ou R, Aodeng G, Ai J. Advancements in the application of the fenton reaction in the cancer microenvironment. Pharmaceutics. 2023;15:8.
127. Xiao J, Guo S, Wang D, An Q. Fenton-like reaction: recent advances and new trends. Chemistry. 2024;30: e202304337.
128. Ren X, Chen D, Wang Y, Li H, Zhang Y, Chen H, Li X, Huo M. Nanozymes-recent development and biomedical applications. J Nanobiotechnology. 2022;20:92.
129. Shi B, Zhang B, Zhang Y, Gu Y, Zheng C, Yan J, Chen W, Yan F, Ye J, Zhang H. Multifunctional gap-enhanced Raman tags for preoperative and intraoperative cancer imaging. Acta Biomater. 2020;104:210–20.
130. Rosenkrans ZT, Ferreira CA, Ni D, Cai W. Internally responsive nanomaterials for activatable multimodal imaging of cancer. Adv Healthc Mater. 2021;10: e2000690.
131. Deng H, Zhang J, Yang Y, Yang J, Wei Y, Ma S, Shen Q. Chemodynamic and photothermal combination therapy based on dual-modified metal-organic framework for inducing tumor ferroptosis/pyroptosis. ACS Appl Mater Interfaces. 2022;14:24089–101.
132. Burke BP, Cawthorne C, Archibald SJ. Multimodal nanoparticle imaging agents: design and applications. Philos Trans A Math Phys Eng Sci. 2017;89:375.
133. Tempany CM, Jayender J, Kapur T, Bueno R, Golby A, Agar N, Jolesz FA. Multimodal imaging for improved diagnosis and treatment of cancers. Cancer. 2015;121:817–27.
134. Fu H, Liu W, Li J, Wu W, Zhao Q, Bao H, Zhou L, Zhu S, Kong J, Zhang H, Cai W. High-Density-Nanotips-Composed 3D Hierarchical Au/CuS hybrids for sensitive, signal-reproducible, and substrate-recyclable SERS Detection. Nanomaterials (Basel). 2022;8:12.
135. Shokrollahi H. Contrast agents for MRI. Mater Sci Eng C Mater Biol Appl. 2013;33:4485–97.
136. Shin MH, Park EY, Han S, Jung HS, Keum DH, Lee GH, Kim T, Kim C, Kim KS, Yun SH, Hahn SK. Multimodal cancer theranosis using hyaluronate-conjugated molybdenum disulfide. Adv Healthc Mater. 2019;8: e1801036.
137. Li W, Rong P, Yang K, Huang P, Sun K, Chen X. Semimetal nanomaterials of antimony as highly efficient agent for photoacoustic imaging and photothermal therapy. Biomaterials. 2015;45:18–26.
138. Li X, Xiu W, Xiao H, Li Y, Yang K, Yuwen L, Yang D, Weng L, Wang L. Fluorescence and ratiometric photoacoustic imaging of endogenous furin activity via peptide functionalized MoS(2) nanosheets. Biomater Sci. 2021;9:8313–22.
139. Meric-Bernstam F, Larkin J, Tabernero J, Bonini C. Enhancing anti-tumour efficacy with immunotherapy combinations. Lancet. 2021;397:1010–22.
140. Zhong YT, Cen Y, Xu L, Li SY, Cheng H. Recent progress in carrier-free nanomedicine for tumor phototherapy. Adv Healthc Mater. 2023;12: e2202307.
141. Zhang C, Hu X, Jin L, Lin L, Lin H, Yang Z, Huang W. Strategic design of conquering hypoxia in tumor for advanced photodynamic therapy. Adv Healthc Mater. 2023;12: e2300530.
142. Pucelik B, Sułek A, Barzowska A, Dąbrowski JM. Recent advances in strategies for overcoming hypoxia in photodynamic therapy of cancer. Cancer Lett. 2020;492:116–35.
143. Qi Y, Yuan Y, Qian Z, Ma X, Yuan W, Song Y. Injectable and self-healing polysaccharide hydrogel loading molybdenum disulfide nanoflakes for synergistic photothermal-photodynamic therapy of breast cancer. Macromol Biosci. 2022;22: e2200161.
144. Fusco L, Gazzi A, Peng G, Shin Y, Vranic S, Bedognetti D, Vitale F, Yilmazer A, Feng X, Fadeel B, et al. Graphene and other 2D materials: a multidisciplinary analysis to uncover the hidden potential as cancer theranostics. Theranostics. 2020;10:5435–88.
145. Li H, Liu M, Zhang S, Xie X, Zhu Y, Liu T, Li J, Tu Z, Wen W. Construction of CpG Delivery Nanoplatforms by Functionalized MoS(2) nanosheets for boosting antitumor immunity in head and neck squamous cell carcinoma. Small. 2023;19: e2300380.
146. Ma Z, Foda MF, Zhao Y, Han H. Multifunctional nanosystems with enhanced cellular uptake for tumor therapy. Adv Healthc Mater. 2022;11: e2101703.

147. Liu J, Lu K, Gao F, Zhao L, Li H, Jiang Y. Multifunctional MoS2 composite nanomaterials for drug delivery and synergistic photothermal therapy in cancer treatment. Ceram Int. 2022;48:22378–86.
148. Raju GSR, Pavitra E, Varaprasad GL, Bandaru SS, Nagaraju GP, Farran B, Huh YS, Han Y-K. Nanoparticles mediated tumor microenvironment modulation: current advances and applications. J Nanobiotechnol. 2022;20:274.
149. Khalid A, Persano S, Shen H, Zhao Y, Blanco E, Ferrari M, Wolfram J. Strategies for improving drug delivery: nanocarriers and microenvironmental priming. Expert Opin Drug Deliv. 2017;14:865–77.
150. Nizzero S, Shen H, Ferrari M, Corradetti B. Immunotherapeutic transport oncophysics: space, time, and immune activation in cancer. Trends Cancer. 2020;6:40–8.
151. Yang S, Li D, Chen L, Zhou X, Fu L, You Y, You Z, Kang L, Li M, He C. Coupling metal organic frameworks with molybdenum disulfide nanoflakes for targeted cancer theranostics. Biomater Sci. 2021;9:3306–18.
152. Imranul-haq M, Lai BF, Chapanian R, Kizhakkedathu JN. Influence of architecture of high molecular weight linear and branched polyglycerols on their biocompatibility and biodistribution. Biomaterials. 2012;33:9135–47.
153. Wang K, Chen Q, Xue W, Li S, Liu Z. Combined chemo-photothermal antitumor therapy using molybdenum disulfide modified with hyperbranched polyglycidyl. ACS Biomater Sci Eng. 2017;3:2325–35.
154. Xu S, Zhong Y, Nie C, Pan Y, Adeli M, Haag R. Co-delivery of doxorubicin and chloroquine by polyglycerol functionalized MoS2 nanosheets for efficient multidrug-resistant cancer therapy. Macromol Biosci. 2021;21: e2100233.
155. Wang S, Wang Y, Jin K, Zhang B, Peng S, Nayak AK, Pang Z. Recent advances in erythrocyte membrane-camouflaged nanoparticles for the delivery of anti-cancer therapeutics. Expert Opin Drug Deliv. 2022;19:965–84.
156. Li JQ, Zhao RX, Yang FM, Qi XT, Ye PK, Xie M. An erythrocyte membrane-camouflaged biomimetic nanoplatform for enhanced chemo-photothermal therapy of breast cancer. J Mater Chem B. 2022;10:2047–56.
157. Murugan C, Lee H, Park S. Tumor-targeted molybdenum disulfide@ barium titanate core-shell nanomedicine for dual photothermal and chemotherapy of triple-negative breast cancer cells. J Mater Chem B. 2023;11:1044–56.
158. Li H, Bruce G, Childerhouse N, Keegan G, Mantovani G, Stolnik S. Biotin receptor-mediated intracellular delivery of synthetic polypeptide-protein complexes. J Control Release. 2023;357:333–41.
159. Song X, Wang R, Gao J, Han X, Jin J, Lv C, Yu F. Construction of a biotin-targeting drug delivery system and its near-infrared theranostic fluorescent probe for real-time image-guided therapy of lung cancer. Chin Chem Lett. 2022;33:1567–71.
160. Chen Z, Wei X, Zheng Y, Zhang Z, Gu W, Liao W, Zhang H, Wang X, Liu J, Li H, Xu W. Targeted co-delivery of curcumin and erlotinib by MoS(2) nanosheets for the combination of synergetic chemotherapy and photothermal therapy of lung cancer. J Nanobiotechnology. 2023;21:333.
161. Shafiee M, Mohamadzade E, ShahidSales S, Khakpouri S, Maftouh M, Parizadeh SA, Hasanian SM, Avan A. Current Status and perspectives regarding the therapeutic potential of targeting EGFR pathway by curcumin in lung cancer. Curr Pharm Des. 2017;23:2002–8.
162. Yamauchi Y, Izumi Y, Yamamoto J, Nomori H. Coadministration of erlotinib and curcumin augmentatively reduces cell viability in lung cancer cells. Phytother Res. 2014;28:728–35.
163. Chiu YJ, Yang JS, Tsai FJ, Chiu HY, Juan YN, Lo YH, Chiang JH. Curcumin suppresses cell proliferation and triggers apoptosis in vemurafenib-resistant melanoma cells by downregulating the EGFR signaling pathway. Environ Toxicol. 2022;37:868–79.
164. Friedrich M, Aigner A. Therapeutic siRNA: State-of-the-Art and Future Perspectives. BioDrugs. 2022;36:549–71.
165. Hu B, Zhong L, Weng Y, Peng L, Huang Y, Zhao Y, Liang XJ. Therapeutic siRNA: state of the art. Signal Transduct Target Ther. 2020;5:101.
166. Zhang J, Zhang T, Gao J. Biocompatible iron oxide nanoparticles for targeted cancer gene therapy: a review. Nanomaterials (Basel). 2022;7:12.
167. Stafford JM, Wyatt MD, McInnes C. Inhibitors of the PLK1 polo-box domain: drug design strategies and therapeutic opportunities in cancer. Expert Opin Drug Discov. 2023;18:65–81.
168. Kou Z, Wang X, Yuan R, Chen H, Zhi Q, Gao L, Wang B, Guo Z, Xue X, Cao W, Guo L. A promising gene delivery system developed from PEGylated MoS2 nanosheets for gene therapy. Nanoscale Res Lett. 2014;9:587.
169. Kong L, Xing L, Zhou B, Du L, Shi X. Dendrimer-modified MoS(2) nanoflakes as a platform for combinational gene silencing and photothermal therapy of tumors. ACS Appl Mater Interfaces. 2017;9:15995–6005.
170. Zhang L, Lu Z, Zhao X. Targeting Bcl-2 for cancer therapy. Biochim Biophys Acta Rev Cancer. 2021;1876: 188569.
171. Tang Q, Chen Y, Li X, Long S, Shi Y, Yu Y, Wu W, Han L, Wang S. The role of PD-1/PD-L1 and application of immune-checkpoint inhibitors in human cancers. Front Immunol. 2022;13: 964442.
172. Yi M, Zheng X, Niu M, Zhu S, Ge H, Wu K. Combination strategies with PD-1/PD-L1 blockade: current advances and future directions. Mol Cancer. 2022;21:28.
173. Ye H, Yan J, Ge C, Wu F, Zhu J, Yin M, Xie L, Zhou Z, Yin L. Tumoral/exosomal PD-L1 silencing reinforces mild photothermal therapy by relieving systemic and local immunosuppression. Chem Eng J. 2024;483: 149093.
174. He X, Zhang S, Tian Y, Cheng W, Jing H. Research progress of nanomedicine-based mild photothermal therapy in tumor. Int J Nanomedicine. 2023;18:1433–68.
175. Ma Y, Liao J, Cheng H, Yang Q, Yang H. Advanced gene therapy system for the treatment of solid tumour: A review. Mater Today Bio. 2024;27: 101138.
176. Zhu X, Li S. Nanomaterials in tumor immunotherapy: new strategies and challenges. Mol Cancer. 2023;22:94.
177. Chen W, Jiang M, Yu W, Xu Z, Liu X, Jia Q, Guan X, Zhang W. CpG-based nanovaccines for cancer immunotherapy. Int J Nanomedicine. 2021;16:5281–99.
178. Rimassa L, Finn RS, Sangro B. Combination immunotherapy for hepatocellular carcinoma. J Hepatol. 2023;79:506–15.
179. Riley RS, June CH, Langer R, Mitchell MJ. Delivery technologies for cancer immunotherapy. Nat Rev Drug Discov. 2019;18:175–96.
180. Han Q, Wang X, Jia X, Cai S, Liang W, Qin Y, Yang R, Wang C. CpG loaded MoS(2) nanosheets as multifunctional agents for photothermal enhanced cancer immunotherapy. Nanoscale. 2017;9:5927–34.
181. Jin Y, Zhuang Y, Dong X, Liu M. Development of CpG oligodeoxynucleotide TLR9 agonists in anti-cancer therapy. Expert Rev Anticancer Ther. 2021;21:841–51.
182. Dongye Z, Li J, Wu Y. Toll-like receptor 9 agonists and combination therapies: strategies to modulate the tumour immune microenvironment for systemic anti-tumour immunity. Br J Cancer. 2022;127:1584–94.
183. Qiao D, Li L, Liu L, Chen Y. Universal and translational nanoparticulate CpG adjuvant. ACS Appl Mater Interfaces. 2022;14:50592–600.
184. Hanagata N. Structure-dependent immunostimulatory effect of CpG oligodeoxynucleotides and their delivery system. Int J Nanomedicine. 2012;7:2181–95.
185. Elmusrati A, Wang J, Wang CY. Tumor microenvironment and immune evasion in head and neck squamous cell carcinoma. Int J Oral Sci. 2021;13:24.
186. Farlow JL, Brenner JC, Lei YL, Chinn SB. Immune deserts in head and neck squamous cell carcinoma: A review of challenges and opportunities for modulating the tumor immune microenvironment. Oral Oncol. 2021;120: 105420.
187. Tang Y, Wang S, Li Y, Yuan C, Zhang J, Xu Z, Hu Y, Shi H, Wang S. Simultaneous glutamine metabolism and PD-L1 inhibition to enhance suppression of triple-negative breast cancer. J Nanobiotechnol. 2022;20:216.
188. Schulte ML, Fu A, Zhao P, Li J, Geng L, Smith ST, Kondo J, Coffey RJ, Johnson MO, Rathmell JC, et al. Pharmacological blockade of ASCT2-dependent glutamine transport leads to antitumor efficacy in preclinical models. Nat Med. 2018;24:194–202.
189. Edwards DN, Ngwa VM, Raybuck AL, Wang S, Hwang Y, Kim LC, Cho SH, Paik Y, Wang Q, Zhang S, et al. Selective glutamine metabolism inhibition in tumor cells improves antitumor T lymphocyte activity in triple-negative breast cancer. J Clin Invest. 2021;78:131.

190. Xu S, Zhang P, Heing-Becker I, Zhang J, Tang P, Bej R, Bhatia S, Zhong Y, Haag R. Dual tumor- and subcellular-targeted photodynamic therapy using glucose-functionalized MoS(2) nanoflakes for multidrug-resistant tumor ablation. Biomaterials. 2022;290: 121844.
191. Li J, Xing Y, Chen X. Intercalating of AlEgens into MoS(2) nanosheets to induce crystal phase transform for enhanced photothermal and photodynamic synergetic anti-tumor therapy. Talanta. 2024;271: 125677.
192. Blau R, Krivitsky A, Epshtein Y, Satchi-Fainaro R. Are nanotheranostics and nanodiagnostics-guided drug delivery stepping stones towards precision medicine? Drug Resist Updat. 2016;27:39–58.
193. Xing R, Zou Q, Yuan C, Zhao L, Chang R, Yan X. Self-assembling endogenous biliverdin as a versatile near-infrared photothermal nanoagent for cancer theranostics. Adv Mater. 2019;31: e1900822.
194. Lu B, Hu S, Wu D, Wu C, Zhu Z, Hu L, Zhang J. Ionic liquid exfoliated Ti(3)C(2)T(x) MXene nanosheets for photoacoustic imaging and synergistic photothermal/chemotherapy of cancer. J Mater Chem B. 2022;10:1226–35.
195. Xia L, Chen J, Xie Y, Zhang S, Xia W, Feng W, Chen Y. Photo-/piezo-activated ultrathin molybdenum disulfide nanomedicine for synergistic tumor therapy. J Mater Chem B. 2023;11:2895–903.
196. Li X, Kong L, Hu W, Zhang C, Pich A, Shi X, Wang X, Xing L. Safe and efficient 2D molybdenum disulfide platform for cooperative imaging-guided photothermal-selective chemotherapy: A preclinical study. J Adv Res. 2022;37:255–66.
197. Movileanu C, Anghelache M, Turtoi M, Voicu G, Neacsu IA, Ficai D, Trusca R, Oprea O, Ficai A, Andronescu E, Calin M. Folic acid-decorated PEGylated magnetite nanoparticles as efficient drug carriers to tumor cells overexpressing folic acid receptor. Int J Pharm. 2022;625: 122064.
198. Thuy LT, Lee S, Dongquoc V, Choi JS. Nanoemulsion Composed of α-Tocopherol Succinate and Dequalinium Shows Mitochondria-Targeting and Anticancer Effects. Antioxidants (Basel). 2023;54:12.
199. Hu W, Xiao T, Li D, Fan Y, Xing L, Wang X, Li Y, Shi X, Shen M. Intelligent molybdenum disulfide complexes as a platform for cooperative imaging-guided tri-mode chemo-photothermo-immunotherapy. Adv Sci (Weinh). 2021;8: e2100165.
200. Lan Y, Liang Q, Sun Y, Cao A, Liu L, Yu S, Zhou L, Liu J, Zhu R, Liu Y. Codelivered chemotherapeutic doxorubicin via a dual-functional immunostimulatory polymeric prodrug for breast cancer immunochemotherapy. ACS Appl Mater Interfaces. 2020;12:31904–21.
201. Wang R, Li N, Zhang T, Sun Y, He X, Lu X, Chu L, Sun K. Tumor microenvironment-responsive micelles assembled from a prodrug of mitoxantrone and 1-methyl tryptophan for enhanced chemo-immunotherapy. Drug Deliv. 2023;30:2182254.
202. Liu J, Zheng J, Nie H, Zhang D, Cao D, Xing Z, Li B, Jia L. Molybdenum disulfide-based hyaluronic acid-guided multifunctional theranostic nanoplatform for magnetic resonance imaging and synergetic chemo-photothermal therapy. J Colloid Interface Sci. 2019;548:131–44.
203. Alsaikhan F. Hyaluronic acid-empowered nanotheranostics in breast and lung cancers therapy. Environ Res. 2023;237: 116951.
204. Cai L, Dong L, Sha X, Zhang S, Liu S, Song X, Zhao M, Wang Q, Xu K, Li J. Exfoliation and in situ functionalization of MoS2 nanosheets for MRI-guided combined low-temperature photothermal therapy and chemotherapy. Mater Des. 2021;210: 110020.
205. Hatami E, Jaggi M, Chauhan SC, Yallapu MM. Gambogic acid: A shining natural compound to nanomedicine for cancer therapeutics. Biochim Biophys Acta Rev Cancer. 2020;1874: 188381.
206. Yon M, Billotey C, Marty JD. Gadolinium-based contrast agents: From gadolinium complexes to colloidal systems. Int J Pharm. 2019;569: 118577.
207. Ghosh S, Yang CJ, Lai JY. Optically active two-dimensional MoS(2)-based nanohybrids for various biosensing applications: A comprehensive review. Biosens Bioelectron. 2024;246: 115861.
208. Ji Y, Wang Y, Wang X, Lv C, Zhou Q, Jiang G, Yan B, Chen L. Beyond the promise: Exploring the complex interactions of nanoparticles within biological systems. J Hazard Mater. 2024;468: 133800.
209. Chrishtop VV, Prilepskii AY, Nikonorova VG, Mironov VA. Nanosafety vs nanotoxicology: adequate animal models for testing in vivo toxicity of nanoparticles. Toxicology. 2021;462:152952.
210. Xiang D, He A, Zhou R, Wang Y, Xiao X, Gong T, Kang W, Lin X, Wang X, Liu L, et al. Building consensus on the application of organoid-based drug sensitivity testing in cancer precision medicine and drug development. Theranostics. 2024;14:3300–16.
211. Jackson CE, Green NH, English WR, Claeyssens F. The use of microphysiological systems to model metastatic cancer. Biofabrication. 2024;16:89654.
212. Jia R, Teng L, Gao L, Su T, Fu L, Qiu Z, Bi Y. Advances in multiple stimuli-responsive drug-delivery systems for cancer therapy. Int J Nanomed. 2021;16:1525–51.
213. Xia M, Luo D, Dong J, Zheng M, Meng G, Wu J, Wei J. Graphene oxide arms oncolytic measles virus for improved effectiveness of cancer therapy. J Exp Clin Cancer Res. 2019;38:408.
214. Cui X, Tang X, Niu Y, Tong L, Zhao H, Yang Y, Jin G, Li M, Han X. Functional phosphorene: Burgeoning generation, two-dimensional nanotherapeutic platform for oncotherapy. Coord Chem Rev. 2024;507: 215744.
215. Yu G-T, Rao L, Wu H, Yang L-L, Bu L-L, Deng W-W, Wu L, Nan X, Zhang W-F, Zhao X-Z, et al. Myeloid-derived suppressor cell membrane-coated magnetic nanoparticles for cancer theranostics by inducing macrophage polarization and synergizing immunogenic. Cell Death. 2018;28:1801389.
216. Su Y, Wang T, Su Y, Li M, Zhou J, Zhang W, Wang W. A neutrophil membrane-functionalized black phosphorus riding inflammatory signal for positive feedback and multimode cancer therapy. Mater Horiz. 2020;7:574–85.
217. He H, Liu L, Morin EE, Liu M, Schwendeman A. Survey of clinical translation of cancer nanomedicines-lessons learned from successes and failures. Acc Chem Res. 2019;52:2445–61.
218. Germain M, Caputo F, Metcalfe S, Tosi G, Spring K, Åslund AKO, Pottier A, Schiffelers R, Ceccaldi A, Schmid R. Delivering the power of nanomedicine to patients today. J Control Release. 2020;326:164–71.
219. Zhang ZW, Yang Y, Wu H, Zhang T. Advances in the two-dimensional layer materials for cancer diagnosis and treatment: unique advantages beyond the microsphere. Front Bioeng Biotechnol. 2023;11:1278871.

Publisher's Note